Multiscale approach incorporating tropocollagen scale to assess the effect of molecular age-related modifications on elastic constants of cortical bone based on finite element and homogenization methods

Marouane El Mouss, Tarek Merzouki, Amna Rekik, Ridha Hambli

Version of Record: https://www.sciencedirect.com/science/article/pii/S1751616122000546
Manuscript_dbfac73c2a350e70adc92e8296580bbb

Multiscale approach incorporating tropocollagen scale to assess the effect of molecular age-related modifications on elastic constants of cortical bone based on finite element and homogenization methods

Marouane EL MOUSS[1], Tarek MERZOUKI[2], Amna REKIK[3], and Ridha HAMBLI[3]

[1]ISCD, Sorbonne Université, 4 place Jussieu, 75252 Paris, France
[2]Univ. de Versailles Saint Quentin en Yvelines, LISV - Versailles Engineering Systems Laboratory, 78140-Vélizy, France
[3]Univ. Orléans, Univ. Tours, INSA CVL, LaMé, 45000 Orléans, France

Corresponding author:
Ridha HAMBLI, Univ. Orléans, Univ. Tours, INSA CVL, LaMé,
8 rue Léonard de Vinci, 45000-Orléans, France.
Email: ridha.hambli@univ-orleans.fr

Abstract:

With osteoporosis and aging, structural changes occur at all hierarchical levels of bone from the molecular scale to the whole tissue, which requires multiscale modeling to analyze the effect of these modifications on the mechanical behavior of bone and its remodeling process. In this paper, a novel hybrid multiscale model for cortical bone incorporating the tropocollagen molecule based on the combination of finite element method and different homogenization techniques was developed. The objective was to investigate the influence of age-related structural alterations that occur at the molecular level, namely the decrease in both molecular diameter (due to the loss of hydration) and number of hydrogen bonds, on mechanical properties of the bone tissue. The proposed multiscale hierarchical approach is divided in two phases: (i) in Step 0, a realistic 3D finite element model for tropocollagen was used to estimate the effective elastic properties at the molecular scale as a function of the collagen molecule's degree of hydration (represented by its external diameter) and the number of its intramolecular hydrogen bonds, and (ii) in Steps 1-10, the effective elastic constants at the higher scales from mineralized fibril to continuum cortical bone tissue were predicted analytically using homogenization equations. The results obtained in healthy mature cortical bone at different scales are in good agreement with the experimental data and multiscale models reported in the literature. Moreover, our model made it possible to visualize the influence of the two parameters (molecular diameter and number of hydrogen bonds) that represent the main age-related alterations at the molecular scale on the mechanical properties of cortical bone, at its different hierarchical levels. **Keywords:** Bone aging, multiscale model, tropocollagen, cortical bone, finite element modeling, homogenization method.

I INTRODUCTION

Bone is a multiscale composite structured tissue extending from a nano-scale level to the whole bone geometry (**Figure 1**) (Habelitz et al., 2002; Hambli, 2011; Raspanti et al., 2001; Rho et al., 1998). The composition of bone and the organization of its constituents give it outstanding mechanical properties. The lowest scale of bone consists primarily of a type I collagen molecule, also called tropocollagen (TC), which gives bone its flexibility, and an inorganic matrix (hydroxyapatite crystals) that gives bone its resilience.

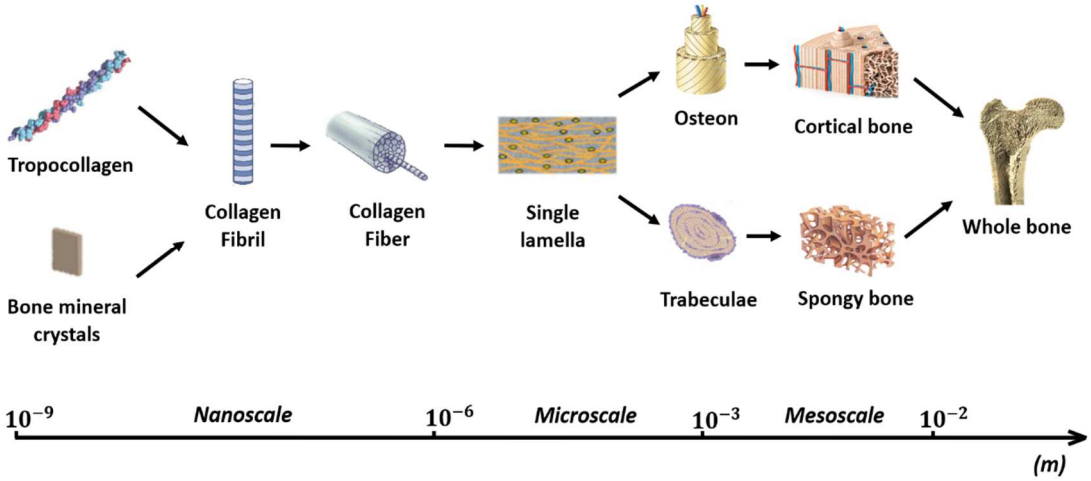

Figure 1: Hierarchical structure of bone.

With osteoporosis, bone aging involves structural changes at all hierarchical levels of bone (Bailey et al., 1998; Barros et al., 2002; Campagnola and Loew, 2003; Chen et al., 2010; Currey, 1969; Mouss et al., 2020; Nagaraja et al., 2007; Saito and Marumo, 2010; Tommasini et al., 2009; Verzár, 1969; Viguet-Carrin et al., 2006; Wallace et al., 2007), which requires multiscale modeling to analyze the effect of aging on the mechanical behavior of bone and its remodeling mechanism.

Several analytical and numerical studies have been performed to address the multiscale modeling of cortical bone's mechanical behavior. Some focused only on certain levels of the bone hierarchy, while others used multi-scale approaches including several levels. However, multiscale models that give a complete description of the hierarchical organization of cortical bone from the molecular scale to the macro-scale level are still lacking.

Among the studies that have focused on a single microscopic scale level, some have described the mechanical behavior of lamellae (Akiva et al., 1998; Vercher et al., 2014; Yoon and Cowin, 2008b), while others have investigated osteons (Ascenzi et al., 2008; Pidaparti et al., 1996; Yoon and Cowin, 2008a). At the submicroscopic scale, just a few models have been developed to estimate the mechanical properties of the mineralized collagen fiber (Yoon and Cowin, 2008b), while most of the studies have been concerned with the mineralized collagen fibrils (Akkus, 2005; Buehler, 2008; Eppell et al., 2006; Ghanbari and Naghdabadi, 2009; Hang and Barber, 2011; Jäger and Fratzl, 2000; Sansalone et al., 2009; Shen et al., 2008; Van Der Rijt et al., 2006; Vercher-Martínez et al., 2015; Yuan et al., 2011). At a lower scale, several studies, mainly based on the finite element (FE) method, have been performed to investigate the mechanical properties of mineralized collagen microfibrils (Barkaoui et al., 2011; Barkaoui and Hambli, 2011, 2014; Barkaoui et al., 2015; Gautieri et al., 2011; Hambli and Barkaoui, 2012). Compared to the previous scales, few modeling studies have focused on the lowest hierarchical level of bone, namely the TC scale. At this molecular scale, the studies based on steered molecular dynamics (SMD) have investigated the mechanical behavior of a single TC molecule under different loading conditions (Buehler, 2006; Gautieri et al., 2009; Lorenzo and Caffarena, 2005), while FE models of the TC have been proposed to study the influence of certain geometrical (Kraiem et al., 2017) and age-related (Mouss et al., 2020) changes on the mechanical properties of the molecule.

On the other hand, bone multiscale modeling has been addressed by many researchers by developing analytical models using homogenization techniques or numerical models.

Based on analytical homogenization methods, some of them have estimated the elastic properties of bone. Two examples are the work of (Hamed et al., 2010) and (Martínez-Reina et al., 2011). The former authors proposed a multiscale model of cortical bone by considering four hierarchical levels: the nanoscale (mineralized fibril), the sub-microscopic scale (lamella), the microstructural level (lamellar structure and osteons), and the mesostructural level (cortical bone). The predicted elastic properties at a lower scale were used as input data for the upper scale. The homogenization method in this model was based on composite laminate theory models for the consideration of constituent orientation at the lamella level, and on the Mori-Tanaka and self-consistent schemes at the other hierarchical levels. In their work, (Martínez-Reina et al., 2011) combined the models proposed by (Yoon and Cowin, 2008a, 2008b) to include the effect of the mineralization process within cortical bone. For this multiscale model, eleven steps and different methods were employed to calculate the stiffness

tensors at different levels. Briefly, the authors used (i) the upper and lower Hill bounds to predict the behavior of elementary constituents (mineral, collagen, and water), (ii) periodic homogenization to account for the periodic distribution of some constituents such as collagen crystals and fibrils, and (iii) the self-consistent scheme for the superposition of osteons and the Mori-Tanaka scheme to include vascular porosity. In the final step, the authors used the theory of poroelasticity to consider the marrow filling pores. Other authors used the analytical homogenization method to predict the fracture toughness of cortical bone (Brynk et al., 2011; Budyn and Hoc, 2010; Fritsch and Hellmich, 2007; Jonvaux et al., 2012). In this regard, (Fritsch et al., 2009) extended their multiscale model (Fritsch and Hellmich, 2007) to present a continuum micromechanics theory for the upscaling of elastoplastic properties. This multiscale model of cortical bone was based on six homogenization steps using the Mori-Tanaka scheme and the self-consistent model.

Studies based on the FE method have also been interested in the multi-scale modeling of bone. As an example, (Barkaoui et al., 2014) proposed a multiscale model to estimate the elastic properties of cortical bone using a hybrid multiscale approach. Their three-phase approach extends the model proposed by (Martínez-Reina et al., 2011) by implementing a 3D FE model of the mineralized collagen microfibril whose mechanical properties were calculated via the neural network method. Another example is that of (Ural and Mischinski, 2013) who developed a multiscale model based on the cohesive FE method to simulate bone fracture at the micro and macroscopic levels. The simulations were performed in three steps: (i) a two-dimensional cortical bone model based on microscopic images, (ii) a simplified three-dimensional cortical bone model with osteons modeled as circular tubes to determine the effect of microscale properties on macroscale fracture toughness, and (iii) an idealized three-dimensional macroscale distal forearm model based on mechanical properties obtained from the microscale model.

In this study, a multi-scale model of bone tissue including all hierarchical levels was developed in order to investigate the effect of age-related structural alterations occurring at the molecular level on the mechanical properties of different bone hierarchical levels. The proposed model is based on two phases. The first phase concerns the molecular scale and is based on the FE method to provide an estimate of the effective mechanical properties of the TC as a function of two parameters affected by bone aging, namely the degree of hydration and the number of hydrogen bonds (H-bonds) (Mouss et al., 2020). This method makes it possible to vary these age-related structural parameters of this elementary constituent and

visualize their influence on the overall mechanical properties of cortical bone, which is difficult using the homogenization equations due to the complex triple helical structure of the TC. Moreover, it may be useful to reproduce other types of collagen molecule structural alterations, such as mutations of H-bonds due to substitutions of residues in certain pathologies (Gautieri et al., 2008), and to study their influence on bone mechanical properties, which is not necessarily accessible with experimental devices. The second phase deals with the higher scales, which were modeled using different micromechanics models published in the literature. The combination of the previous two phases allows us to evaluate the macroscopic elastic properties of the cortical bone, and to investigate the influence of some age-related molecular modifications on the mechanical properties of its different levels.

II MATERIALS AND METHODS

The proposed step-by-step model to estimate the effective elastic properties of bone at different scales is based on an algorithm composed of **11 steps** built in **2 phases** (**Figure 2**).

Collagen, together with hydroxyapatite (HA crystals) and water, constitute the elementary components of bone tissue. **The first phase (Step 0)** is based on our previous work on the study of the effect of hydration and number of H-bonds within the collagen molecule on the mechanical properties of the TC. It consists in using FEM and DOE methods to estimate the stiffness matrix of the collagen molecule as a function of its degree of hydration (represented by its external diameter) and the number of intramolecular H-bonds. This first phase represents in large part the originality of the proposed multiscale model. To the best of our knowledge, none of the proposed multiscale models in the literature incorporate a 3D FE model of TC to consider the effect of structural alterations, which occur at the molecular scale, on the macroscopic bone mechanical properties. In this study, we will focus mainly on the age-related alterations in osteoporosis.

The second phase includes 10 analytical homogenization steps based on several methods in the literature to estimate elastic properties at each scale of the hierarchical structure of cortical bone (Barkaoui et al., 2014; Hamed et al., 2010; Martínez-Reina et al., 2011; Yoon and Cowin, 2008a, 2008b): considering the water embedded in the space between collagen molecules and the fact that these molecules are linked through *cross-links*, **Step 1** consists in determining the elastic constants of the collagen-water composite using the (Mori and Tanaka, 1973) scheme. Then, the method of (Nemat-Nasser and Hori, 2013) for composites with periodically distributed inclusions is applied in **Steps 2, 3, and 4** to calculate the stiffness tensor of collagen fibrils (composed of HA crystals surrounded by cross-linked collagen), fibers (composed of fibrils surrounded by extra-fibrillar mineral), and lamellae (fibers surrounded by extra-fibrillar mineral). The method of (Nemat-Nasser and Hori, 2013) is also used in **Step 5** to calculate the stiffness tensor of the lamellae with canaliculi, which were simplified as straight tubes oriented in three directions within the osteon: radial, longitudinal, and circumferential. Three different laminate structures were considered to take into account each type of canaliculus. In **Step 6**, the stiffness tensor of a material that comprises the three types of the canaliculi is obtained by a laminate-specific homogenization method developed by (Chou et al., 1972). In **Step 7**, the lacunar porosity is introduced into the model in the same way as the canalicular porosity in step 5, simply by changing the pore shape. In **Step 8**, a symmetrization technique is used to estimate the effective transversely

isotropic elastic constants of a single osteon, given its approximately cylindrical shape. The cortical tissue is considered as a composite formed by the interpenetration of osteons with different mineral content as a consequence of bone remodeling. Therefore, the stiffness tensor of this new composite is estimated in **Step 9** using the self-consistent scheme to take into account the superimposition of these phases of osteons. Finally, in **Step 10**, a Mori-Tanaka scheme with diluted inclusions representing the Haversian canals is used to include vascular porosity in the model.

Erreur ! Source du renvoi introuvable.

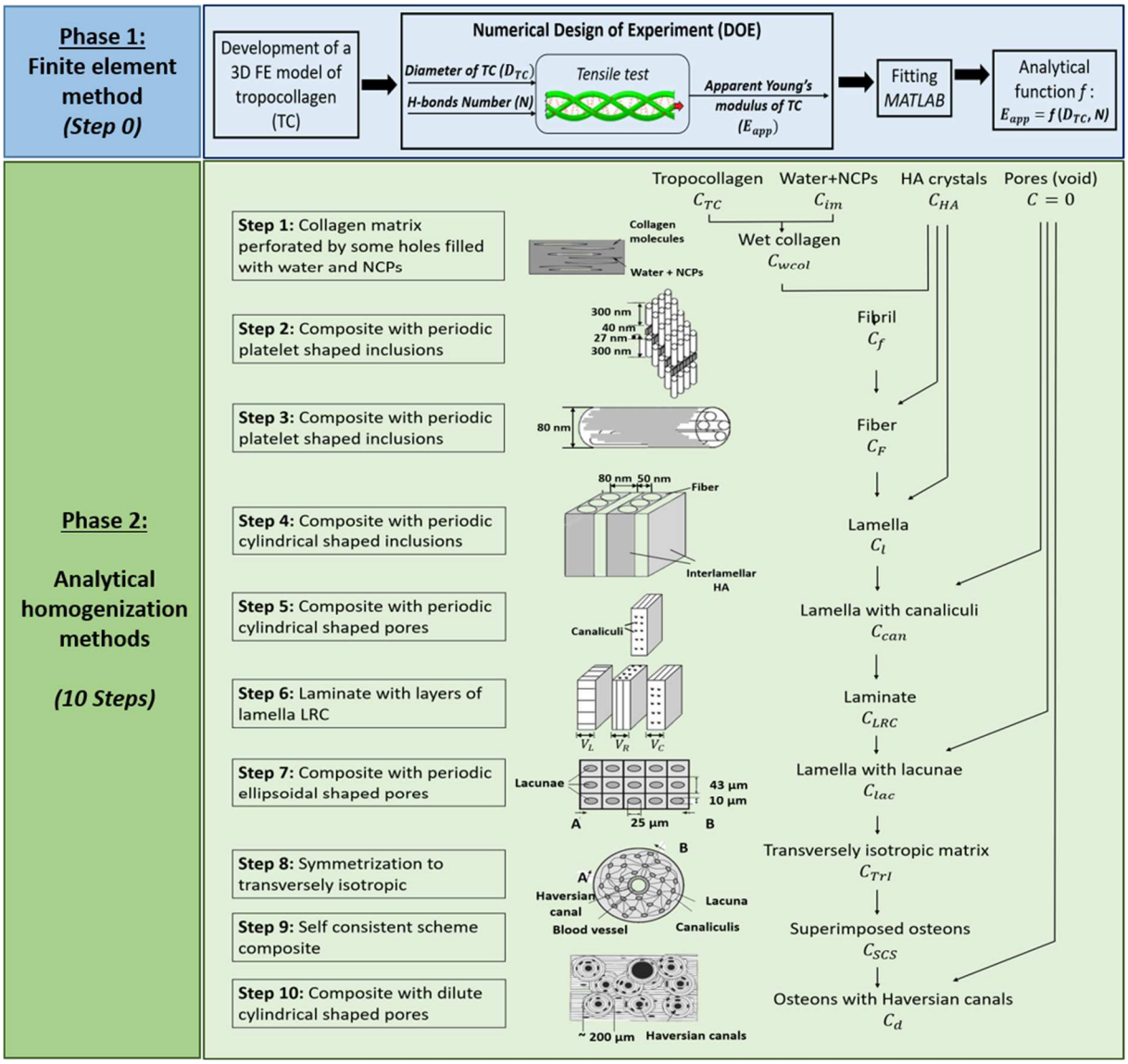

Figure 2: Overview of the algorithm used for estimating the elastic properties of cortical tissue. The illustrations in phase2 are from the work of (Hamed et al., 2010; Martínez-Reina et al., 2011; Yoon and Cowin, 2008a, 2008b).

II.1 Step 0: tropocollagen molecule

This section describes how the effective stiffness matrix of the organic elementary component of bone tissue, namely the TC molecule, was estimated. This step is based on the work of (Mouss et al., 2020) and presents three principal stages: (i) the development of a realistic 3D model of type I TC, taking into account the intramolecular H-bonds between the three polypeptide chains of the triple helix, (ii) the performance of a numerical design of experiments (DOE) for the variations in the degree of hydration (represented by the external diameter) of the TC and the number of H-bonds, and (iii) the estimate of an analytical function (f) linking the mechanical properties (the apparent Young's modulus E_{app}) of the collagen molecule to the previous two parameters (degree of hydration and H-bond number).

II.1.1 3D finite element modeling

Before describing the 3D FE model of the TC, it is necessary to provide a brief description of the components of this molecule.

Type I collagen molecules are rod-like structures with a length of about 300 nm and a diameter of 1.5 nm composed of three α-chains, which twist tightly around each other to form a right handed triple-stranded superhelix with a pitch of ~ 8.6 nm (**Figure 3**). The formation of H-bonds between the three helical polypeptide chains stabilizes the triple helix (Bhagavan, 2001; Bhattacharjee and Bansal, 2008; Ramachandran and Kartha, 1955; Ramachandran, 1956; Ramachandran and Kartha, 1954).

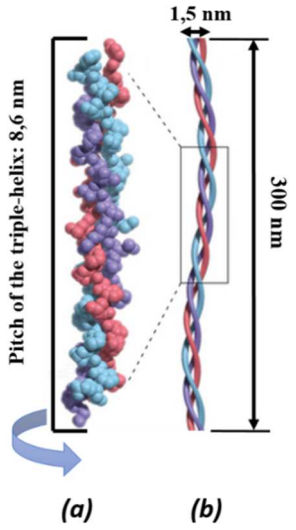

Figure 3: Tropocollagen molecule: The pitch of the triple-helix is about 8.6 nm (a), its length and diameter are 300 and 1.5 nm respectively (b).

Each of the three α-chains forms a left-handed helix with approximately three amino acid residues per turn and a rise per residue along the helical axis of 3 Å. These chains are characterized by a series of $Gly - X - Y$ repeats where X and Y can accommodate any type of amino acids. The stability of the triple helix depends on residues in the X and Y positions (Persikov et al., 2000). Polypeptide chains consisting of proline (Pro) and hydroxyproline (Hyp) residues in the X and Y positions respectively form an extremely stable triple helix (**Figure 4**). The α-chains are also characterized by amino $(N) -$ and carboxy $(C) -$terminal propeptide sequences, which flank the series of $Gly - X - Y$. The TC structure is stabilized by a direct $N - H\ (GLY) \cdots O = C$ (X position) inter-chain H-bond for all sequences (Bella et al., 1994; Privalov, 1982). The existence and the importance of these intramolecular links in stabilizing the TC conformation and assembly have been widely studied and confirmed using different approaches (Bella et al., 1994; Brodsky and Ramshaw, 1997; Fratzl and Weinkamer, 2007; Gautieri et al., 2008; Privalov, 1982).

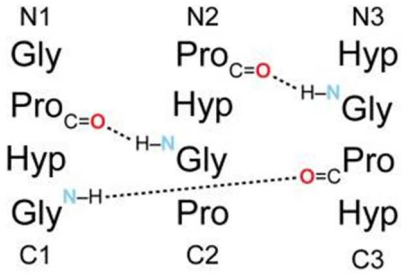

Figure 4: Periodic arrangement of interchain NH...OC hydrogen bonds within the triple helix (Shoulders and Raines, 2009).

(Mouss et al., 2020) developed a 3D FE model for the TC molecule taking into account the intramolecular H-bonds between helices to study the influence of molecular diameter and H-bond number on the elastic modulus of the collagen molecule. The three α-chains in the proposed model were approximated by continuous helices, and assumed to have an isotropic elastic behavior. The inter-chain H-bonds that connect the NH of Gly in a chain to the CO of the residue in the position X of the neighboring chain were modeled using calibrated linear elastic elements *(Spring elements*). Localization of the residues was carried out using their coordinates, which were calculated based on the parametric equations of each helix of the FE model and the axial distance between two residues. The elastic properties of the α-chains and the tensile stiffness of the spring elements were based on the available data in the literature. The 3D geometry model was meshed using about 9000 hexahedral linear elements of type C3D8 and solved via the ABAQUS standard scheme. This discretization of

the model was chosen from a convergence study by varying the density of the mesh (**Figure 5**).

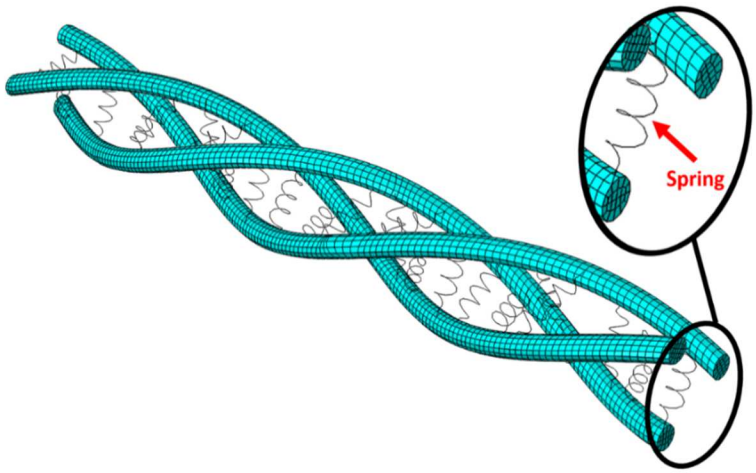

Figure 5: Mesh of the 3D finite element model of tropocollagen (The spring elements are the representation of H-bonds).

II.1.2 Parametric study (DOE)

Along with osteoporosis, bone aging involves structural changes at all hierarchical scales of bone (Bailey et al., 1998; Barros et al., 2002; Campagnola and Loew, 2003; Chen et al., 2010; Currey, 1969; Nagaraja et al., 2007; Saito and Marumo, 2010; Tommasini et al., 2009; Verzár, 1969; Viguet-Carrin et al., 2006; Wallace et al., 2007). Particularly at the molecular level, two main age-related structural alterations occur within the TC, namely the change in diameter (due to the change in the degree of hydration of the molecule) and the change in the number of H-bonds (Bailey et al., 1998; Barros et al., 2002; Eklouh-Molinier et al., 2015; Verz et al., 1963; Verzár, 1969). It has been suggested that a weakening of water/ TC interactions occurs with age, resulting in a loss of hydration of the molecule and a corresponding decrease in its diameter (Bella et al., 1995). Moreover, heat denaturation experiments showed that H-bonds in the collagen molecule decrease with age (Verzár, 1969) confirmed by (Verz et al., 1963) who observed a higher frequency of H-bonds in the collagen molecule of young tendons compared with older ages. Therefore, the objective of the parametric study was to use the previously developed TC FE model to identify an analytical relationship between these two parameters affected by aging and the mechanical properties (in terms of Young's modulus) of the macromolecule. In order to establish this analytical relationship a numerical factorial DOE of two factors was performed (**Figure 6**).

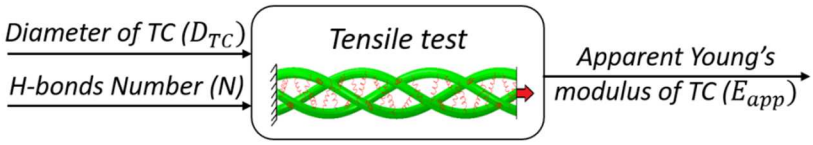

Figure 6: Schematic representation of the numerical parametric study.

Depending on the degree of hydration, numerical simulations were carried out for various diameters D_{TC} = 1, 1.23, and 1.5 nm, which correspond to the dry, semi-wet and wet states of the TC, respectively (Charvolin and Sadoc, 2012; Cusack and Miller, 1979; Gautieri et al., 2009; Harley et al., 1977; Sasaki and Odajima, 1996). The H-bond number was chosen to vary from 0, corresponding to the case of unlinked helices, to 30 corresponding to the average number of H-bonds in an ideal collagen segment of about 8 nm in length (Bella et al., 1994; Gautieri et al., 2008; Lorenzo and Caffarena, 2005; Persikov et al., 2000; Vesentini et al., 2005). The other geometrical parameters (length and pitch of the molecule as well as the diameter of the helices) were not modified during this parametric study.

The apparent Young's modulus of the TC is the primary response of this DOE. To evaluate this parameter, tensile loads were applied along the axial direction of the triple helix for different combinations of diameter and number of H-bonds in small-scale strain ($\leq 10\%$). The tensile test provides a "force-displacement" curve, which allows the local Young's modulus E(d) to be assessed (in terms of deformation) by applying the following relation derived from continuum mechanical theories (Buehler and Wong, 2007):

$$E_{app}(d) = \frac{d_0}{A_{TC}} \frac{\partial F(d)}{\partial d} \qquad \text{(Eq.1)}$$

where d_0 is the initial undeformed length of the collagen molecule, A_{TC} denotes the equivalent cross-sectional area of a collagen molecule assuming a cylindrical shape of diameter (D_{TC}), and F is the magnitude of stretching load.

The apparent Young's modulus was then determined as the tangential slope corresponding to 10% tensile strain (Buehler, 2006).

II.1.3 Results of the DOE

The results of the parametric study, i.e., the values predicted by the proposed FE model of the apparent Young's modulus for each combination of molecular diameter and number of H-bonds, are represented in **Figure 7** in the two-dimensional domain (D_{TC}, N).

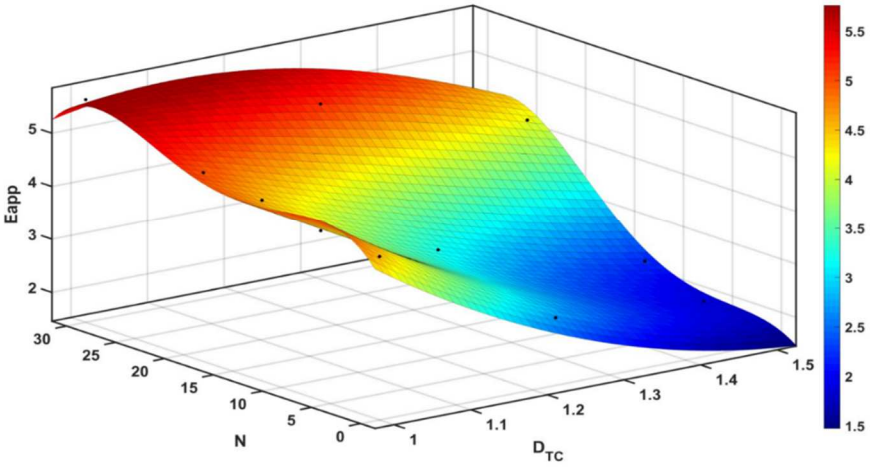

Figure 7: Apparent Young's modulus as a function of H-bonds and molecular diameter (response surface).

The surface response $E_{app} = f(D_{TC}, \mathrm{N})$ was constructed using polynomial approximation. The nonlinear model of the approximated function (f) can be written in the following form:

$$f = \alpha_0 + \sum_{i=1}^{n} \alpha_i x_i + \sum_{i=1}^{n} \alpha_{ii} x_i^2 + \sum_{i<j}^{n} \alpha_{ij} x_i x_j + \sum_{i=1}^{k} \beta_{ii} x_i^3 + \sum_{\substack{i=1 \\ i \neq j}}^{n} \beta_{ij} x_i^2 x_j + \sum_{i=1}^{n} \gamma_{ii} x_i^4 + \sum_{\substack{i=1 \\ i \neq j}}^{n} \gamma_{ij} x_i^3 x_j + \prod_{i=1}^{n} \xi x_i^2 + \varepsilon \qquad \text{(Eq.2)}$$

where k=1 and n=2; the variables x_1 and x_2 denote N and D_{TC}, respectively, $\{\alpha, \beta, \gamma, \xi\}$ are the regression coefficients; and ε is the error of the approximation. The regression coefficients in (Eq.2) were determined using the curve fitting tool in MATLAB software. The obtained constants are summarized in **Table 1**.

Table 1: Coefficients of the approximated polynomial function.

Coefficients	α_0	α_1	α_2	α_{11}	α_{12}	α_{22}	β_{11}	β_{12}	β_{21}	γ_{11}	γ_{12}	ξ
Values	**22.01**	**0.2138**	**-25.44**	**-0.06821**	**-0.03195**	**7.928**	**0.001816**	**0.06027**	**-0.03344**	**$-2.551.10^{-5}$**	**$-3.4.10^{-4}$**	**-0.01696**

Step 0 provides the approximate analytical function $E_{app} = f(D_{TC}, \mathrm{N})$, which is used to determine the stiffness matrix of collagen, the elementary organic component of bone tissue. The other two elementary bone components are hydroxyapatite (HA) and water-NPCs. The stiffness matrices of these two components were defined from the elastic properties available in the literature (**Table 2**). For simplicity, all elementary components are assumed to have an isotropic linear elastic behavior. The following steps of the multiscale model development are based on different analytical homogenization methods mainly inspired by the work of (Martínez-Reina et al., 2011), which we have slightly modified. The proposed approach includes ten steps starting with Step 1 representing the matrix of cross-linked collagen molecules up to Step 10 representing the cortical bone.

II.2 Step 1: *Cross-linked* collagen

Unlike (Martínez-Reina et al., 2011), who used Voigt and Reuss bounds to estimate the effective mechanical properties at the nanostructural level, we assume that a continuous approach is applicable at this scale. This assumption has been made by several researchers, and the fact that collagen molecules are linked through cross-links has motivated the use of a continuous matrix containing some holes filled with water and NPCs (Fritsch and Hellmich, 2007; Fritsch et al., 2009; Hamed et al., 2010; Hellmich et al., 2004; Hellmich and Ulm, 2002). The holes are represented as cylindrical inclusions (inhomogeneities). The Mori-Tanaka scheme (Benveniste, 1987; Mori and Tanaka, 1973) was used to estimate the effective stiffness tensor of the bone at this scale. Subscripts "TC" and "w" refer to collagen and water with NPCs, respectively. Given the stiffness tensors of collagen, $\mathbf{C}_{TC}$, and water-NPCs, $\mathbf{C}_w$, the effective stiffness tensor of the collagen-water composite, $\mathbf{C}_{wcol}$ is obtained as:

$$\mathbf{C}_{wcol} = \mathbf{C}_{TC} + \phi_w[(\mathbf{C}_w - \mathbf{C}_{TC}) : \mathbf{A}] : [(1-\phi_w)\,\mathbf{I} + \phi_w\,\mathbf{A}] \qquad \text{(Eq.3)}$$

where $\mathbf{A} = \left[\mathbf{I} + \mathbf{S}_{ell} : \mathbf{C}_c^{-1} : (\mathbf{C}_w - \mathbf{C}_c)\right]^{-1}$ is the strain concentration tensor for a single ellipsoidal inclusion in an infinite elastic matrix, $\mathbf{I}$ is the identity tensor, and $\mathbf{S}_{ell}$ is the Eshelby tensor which depends on the elastic properties of the matrix and on the cylindrical shape of inclusions (see *Appendix B*). ϕ_w is the volume fraction of water and NPCs in the cross-linked collagen.

II.3 Step 2: Mineralized collagen fibril

In this step, the mineralized collagen fibril is considered as a composite in which the *cross-linked* collagen molecules (matrix) embed platelet-shaped crystals (inclusions), which are assumed to be periodically distributed along the axes of the *cross-linked* collagen molecules. Therefore, the method of (Nemat-Nasser and Hori, 2013) was used to calculate the effective stiffness tensor of this composite with periodically distributed inclusions:

$$\mathbf{C}_f = \mathbf{C}_{wcol}\left\{1 - \phi_{ha}\left[(\mathbf{C}_{wcol} - \mathbf{C}_{ha})^{-1}.\,\mathbf{C}_{wcol} - \mathbf{P}_{p,wcol}\right]^{-1}\right\} \qquad \text{(Eq.4)}$$

where $\mathbf{C}_f$ is the effective stiffness tensor of the mineralized collagen fibril, $\mathbf{C}_{ha}$ is the stiffness tensor of the HA crystals (intrafibrillar mineral) and $\mathbf{C}_{wcol}$ is the tensor of the collagen-water composite obtained in Step 1. ϕ_{ha} is the volumetric fraction of platelet shaped mineral crystals in the composite and $\mathbf{P}_{p,wcol}$ is a periodic tensorial operator for platelet-shaped inclusions of mineral crystals in a *cross-linked* collagen matrix (see *Appendix C*).

II.4 Step 3: Mineralized collagen fiber

The collagen fiber is assumed as a composite with periodically distributed cylindrical inclusions (collagen fibrils) that are embedded in an extrafibrillar mineral matrix. Depending on the made assumption about the arrangement of HA crystals in the extra-fibrillar matrix, different homogenization schemes have been used in the literature to calculate the elastic constants $\mathbf{C}_{wha}$ of this matrix. Some assumed that the extra-fibrillar mineral crystals are closely packed and adhere strongly to the fibril surface (Hassenkam et al., 2004; Sasaki and Sudoh, 1997; Zhang et al., 2003), and therefore they presented it as a continuous HA matrix with a small volume fraction of void spaces filled with water and NPCs. In this case, the Mori-Tanaka method is an appropriate choice to obtain the effective elastic properties of the extra-fibrillar HA matrix. Others have assumed that the extra-fibrillar mineral crystals are dispersed and highly disordered (Fratzl et al., 1996; Lees et al., 1994; Rosen et al., 2002), and thus the extra-fibrillar HA matrix was considered as a porous polycrystal consisting of HA crystals with intercrystalline pores in-between filled with water and NPCs (Fritsch et al., 2009; Hellmich et al., 2004). In this case, a self-coherent scheme (Budiansky, 1965; Hill, 1963) with two interpenetrating phases, namely HA crystals and pores filled with water and NPCs, was used to capture the overall behavior of the extra-fibrillar matrix (Fritsch et al., 2009; Hellmich et al., 2004).

With our model, we have assumed the first hypothesis which justifies the choice of the Mori-Tanaka scheme to estimate the stiffness matrix $\mathbf{C}_{wha}$ of the extra-fibrillar mineral HA:

$$\mathbf{C}_{wha} = \mathbf{C}_{ha} + \phi'_w \left[(\mathbf{C}_w - \mathbf{C}_{ha}) : \mathbf{A}\right] : \left[(1-\phi'_w)\,\mathbf{I} + \phi'_w\,\mathbf{A}\right]$$
$$\mathbf{A} = \left[\mathbf{I} + \mathbf{S}_{sph} : \mathbf{C}_{ha}^{-1} : (\mathbf{C}_w - \mathbf{C}_{ha})\right]^{-1} \quad \text{(Eq.5)}$$

where the subscripts "w" and "ha" refer to water-NPCs and extrafibrillar HA crystals, respectively.

$\mathbf{I}$ is the identity tensor and $\mathbf{S}_{sph}$ is the Eshelby tensor which depends on the elastic properties of the matrix and on the spherical shape of inclusions (see *Appendix B*).

The effective stiffness tensor of the fiber $\mathbf{C}_F$ is estimated by employing an analogous expression to the one previously used for the fibril in Step 3 (Martínez-Reina et al., 2011; Nemat-Nasser and Hori, 2013):

$$\mathbf{C}_F = \mathbf{C}_{wha}\left\{1 - \phi_f\left[(\mathbf{C}_{wha} - \mathbf{C}_f)^{-1}.\mathbf{C}_{wha} - \mathbf{P}_{c,wha}\right]^{-1}\right\} \quad \text{(Eq.6)}$$

ϕ_f is the volumetric fraction of fibrils within the fiber. $\mathbf{P}_{c,wha}$ is a periodic operator, corresponding to infinite cylindrical periodic inclusions of fibrils embedded in an extra-fibrillar mineral matrix with the stiffness tensor $\mathbf{C}_{wha}$ (see *Appendix C*).

II.5 Step 4: Lamella

In the same way as the fiber, the effective stiffness tensor of the lamella, $\mathbf{C}_l$, is estimated by assuming that the lamella is a composite with a matrix of extrafibrillar mineral and periodically distributed cylindrical inclusions of fibers (Nemat-Nasser and Hori, 2013):

$$\mathbf{C}_l = \mathbf{C}_{wha}\left\{1 - \phi_F\left[(\mathbf{C}_{wha} - \mathbf{C}_F)^{-1}.\mathbf{C}_{wha} - \mathbf{P}_{c,wha}\right]^{-1}\right\} \quad \text{(Eq.7)}$$

where ϕ_F is the volumetric fraction of fibers and $\mathbf{P}_{c,wha}$ the same operator as in Step 3.

II.6 Step 5: Lamella with canaliculi

The aim of this step is to include the canalicular porosity. The canaliculi are assumed as infinite cylindrical periodically distributed voids. These voids (inclusions) or 'pores' have a null stiffness (Martínez-Reina et al., 2011). Thus, the stiffness tensor of a lamella with canaliculi $\mathbf{C}_{can}$ takes the form (Nemat-Nasser and Hori, 2013):

$$\mathbf{C}_{can} = \mathbf{C}_l \left\{1 - p_{can} \left(\mathbf{I} - \mathbf{P}_{c,l}\right)^{-1}\right\} \qquad \text{(Eq.8)}$$

where p_{can} is the canalicular porosity and $\mathbf{P}_{c,l}$ the periodic operator for infinite cylindrical inclusions in a matrix of lamellar tissue (see *Appendix C*).

II.7 Step 6: Laminate with lamellae LRC

(Beno et al., 2006) sorted the canaliculi in osteons into three directions: longitudinal (L), radial (R), and circumferential (C). On the other hand, (Yoon and Cowin, 2008a) identified these directions with the lamellar orthotropy directions. Thus, with the previous equation (Eq.8) and using the appropriate periodic operator $\mathbf{P}_{c,l}$, it is possible to estimate $\mathbf{C}_{can}$ for three types of laminates (L, R and C). The only difference between these laminates is the direction of the canaliculi, which is taken into account in the operator $\mathbf{P}_{c,l}$ of (Eq.8) . The components of the effective stiffness tensor of a laminate $(\mathbf{C}_{LRC})$ composed of three layers is calculated following (Chou et al., 1972):

$$(\mathbf{C}_{LRC})_{ij} = \sum_{k=1}^{3} \mathrm{V}^k \left[(\mathbf{C}_{can}{}^k)_{ij} - \frac{(\mathbf{C}_{can}{}^k)_{i3} (\mathbf{C}_{can}{}^k)_{i3}}{(\mathbf{C}_{can}{}^k)_{33}} + \frac{(\mathbf{C}_{can}{}^k)_{i3} \sum_{\Omega=1}^{3} \frac{V^{\Omega} (\mathbf{C}_{can}{}^{\Omega})_{j3}}{(\mathbf{C}_{can}{}^{\Omega})_{33}}}{(\mathbf{C}_{can}{}^{\Omega})_{33} \sum_{\Omega=1}^{3} \frac{\mathrm{V}^{\Omega}}{(\mathbf{C}_{can}{}^{\Omega})_{33}}} \right] \qquad \text{(Eq.9)}$$

where $i, j \in \{1, 2, 3 \; or \; 6\}$, and V^k is the volume fraction of the layer, where the indices $k = 1, 2, 3$ correspond to L, R, C.

If $i = 1, 2, 3$ or 6 and $j = 4$ or 5, then $(\mathbf{C}_{LRC})_{ij} = (\mathbf{C}_{LRC})_{ji} = 0$. Finally, if i and j are 4 or 5, the components are:

$$(\mathbf{C}_{LRC})_{ij} = \frac{\sum_{k=1}^{3} \frac{\mathrm{V}^k}{\Delta_k} (\mathbf{C}_{can}{}^k)_{ij}}{\sum_{k=1}^{3} \sum_{\Omega=1}^{3} \frac{\mathrm{V}^k \mathrm{V}^{\Omega}}{\Delta_k \Delta_{\Omega}} \Gamma_{k\Omega}} \qquad \text{(Eq.10)}$$

where $\Delta_k = \left(\mathbf{C}_{can}{}^{k}\right)_{44}\left(\mathbf{C}_{can}{}^{k}\right)_{55} - \left(\mathbf{C}_{can}{}^{k}\right)_{45}\left(\mathbf{C}_{can}{}^{k}\right)_{54}$

and $\Gamma_{k\Omega} = \left(\mathbf{C}_{can}{}^{k}\right)_{44}\left(\mathbf{C}_{can}{}^{\Omega}\right)_{55} - \left(\mathbf{C}_{can}{}^{k}\right)_{45}\left(\mathbf{C}_{can}{}^{\Omega}\right)_{54}$

II.8 Step 7: Lamellae with lacunae

At this step, lacunar porosity is included in the lamella layers assuming that the lacunae are periodically distributed ellipsoids (Martínez-Reina et al., 2011).

The stiffness tensor of the lamellae with lacunae, $\mathbf{C}_{lac}$, is estimated by an equation similar to (Eq.8):

$$\mathbf{C}_{lac} = \mathbf{C}_{LRC}\left\{1 - p_{lac}\,(1 - \mathbf{P}_{e,LRC})^{-1}\right\} \qquad \text{(Eq.11)}$$

where p_{lac} is the lacunar porosity and $\mathbf{P}_{e,LRC}$ is the periodic operator for ellipsoidal inclusions in a matrix of laminate LRC. This periodic operator (Nemat-Nasser and Hori, 2013) and the ellipsoidal lacunae dimensions (Remaggi et al., 1998) are given in *Appendix C*.

II.9 Step 8: Single osteon

The effective stiffness tensor of the osteon, $\mathbf{C}_{TrI}$, was estimated using the method presented in (Yoon et al., 2002) and (Martínez-Reina et al., 2011). This method consists in constructing the effective upper and lower bounds of the effective transversely isotropic elastic constants using the known orthotropic values. Since the upper and lower bounds are generally very close, this method allows the mean value to be used as an estimate of the transversely isotropic elastic constants of the osteon. This symmetrization step provides an estimate of the stiffness tensor of a single osteon, $\mathbf{C}_{TrI}$, where the subscript (TrI) stands for transversely isotropic.

II.10 Step 9: Superposition of osteons

In adults, most of the cortical tissue is secondary lamellar bone, in which osteons interpenetrate each other. Osteons may have different mineral contents: newly formed osteons (phase a), with a low mineral content and old osteons (phase b) with a high mineral content. The objective of this step is to superimpose these two types of osteons. A self-consistent scheme was used (Hill, 1963), according to Martínez (Martínez-Reina et al., 2011):

$$\mathbf{C}_{SCS} = \Big\{\phi_a\,\mathbf{C}^{a}_{TrI}\left[1 + \mathbb{P}_{cyl}\left(\mathbf{C}^{a}_{TrI} - \mathbf{C}_{SCS}\right)\right]^{-1} + (1 - \phi_a)\mathbf{C}^{b}_{TrI}\left[1 + \mathbb{P}_{cyl}\left(\mathbf{C}^{b}_{TrI} - \mathbf{C}_{SCS}\right)\right]^{-1}\Big\}. \qquad \text{(Eq.12)}$$

$$\left\{\phi_a \left[1 + \mathbb{P}_{cyl} \left(\mathbf{C}_{TrI}^{a} - \mathbf{C}_{SCS}\right)\right]^{-1} + (1 - \phi_a) \left[1 + \mathbb{P}_{cyl} \left(\mathbf{C}_{TrI}^{b} - \mathbf{C}_{SCS}\right)\right]^{-1}\right\}^{-1}$$

where $\mathbf{C}_{SCS}$, $\mathbf{C}_{TrI}^{a}$ and $\mathbf{C}_{TrI}^{b}$ are, respectively, the stiffness tensors of the composite (secondary lamellar tissue), phase a (newly formed osteons) and phase b (mature osteons). These two tensors are obtained by the previous steps (from Step 1 to Step 8) starting from different mineral contents. ϕ_a is the volume fraction of newly formed osteons and $\mathbb{P}_{cyl}$ is the Hill polarization tensor for cylindrical inclusions corresponding to the shape of the osteons. This tensor is related to both the Eshelby tensor $\boldsymbol{S}_{cyl}$ (see *Appendix B*) and the stiffness tensor of the matrix by (Suvorov and Dvorak, 2002): $\boldsymbol{S}_{cyl} = \mathbb{P}_{cyl}\, \boldsymbol{C}_{TrI}^{b}$. (Eq.12) is solved iteratively with the following initial value: $\mathbf{C}_{SCS}{}^{0} = \mathbf{C}_{TrI}^{b}$.

II.11 Step 10: Drained cortical tissue

In this last step, vascular porosity was introduced to estimate the stiffness tensor of the cortical tissue, $\mathbf{C}_d$. For this purpose, Benveniste's (Benveniste, 1987) interpretation of Mori-Tanaka's approach for void inclusions was used (Martínez-Reina et al., 2011):

$$\mathbf{C}_d = \mathbf{C}_{TrI} \left[1 + \frac{p_{vas}}{1 - p_{vas}} \left(1 - \mathbf{S}_{cyl}\right)^{-1}\right]^{-1} \qquad \text{(Eq.13)}$$

where p_{vas} is the vascular porosity (Haversian canals). The Eshelby tensor $\mathbf{S}_{cyl}$, as stated earlier, is the one corresponding to cylindrical inclusions in a transversely isotropic matrix.

II.12 Model parameters

In the same way as other composite materials, the overall mechanical behavior of bone is strongly affected by the mechanical properties and the volume fraction of its elementary components. A wide range of values for these mechanical properties has been reported in the literature. The values chosen in our model are shown in **Table 2**. Note that the Young's modulus of collagen is given by the analytical function, approximated in Step 0, as a function of the hydration state of the molecule (represented by its diameter) and the number of H-bonds.

Table 2: Mechanical properties and volume fractions of selected bone elementary components in our model (Hamed et al., 2010; Martínez-Reina et al., 2011). Superscripts "a" and "b" denote the values used in newly formed and mature osteons, respectively. The non-indexed values are fixed.

Component	Elastic modulus (GPa)	Poisson's ratio	Volume fraction
Collagen	$E_{app} = f(D_{TC}, \mathrm{N})$	0.35	0.354
HA crystals	114	0.28	0.163^a 0.418^b
Water-NPCs	0.138	0.49	0.483^a 0.228^b

It should also be noted that two volume fractions for HA crystals were selected to distinguish newly formed osteons from more mineralized mature osteons. Finally, we note that the volume fractions (ϕ) used in the different homogenization steps of the model were estimated based on the work of (Martínez-Reina et al., 2011). The calculated values are summarized in **Table 3**.

Table 3: Different volume fractions used in the model (Martínez-Reina et al., 2011; Yoon and Cowin, 2008a). Superscripts "a" and "b" denote the values used in newly formed and mature osteons, respectively. The non-indexed values are fixed.

Volume fraction	Value
Water-NPCs in the cross-linked collagen ($\boldsymbol{\phi_w}$)	0.27^a 0.14^b
HA crystals in the fibril ($\boldsymbol{\phi_{ha}}$)	0.09^a 0.22^b
Water-NPCs in the HA extrafibrillar matrix ($\boldsymbol{\phi'_w}$)	0.39^a 0.36^b
Fibrils within the fiber ($\boldsymbol{\phi_f}$)	0.58
Fibers within the lamella ($\boldsymbol{\phi_F}$)	0.91
Canalicular porosity ($\boldsymbol{p_{can}}$)	0.0418
Type L lamellae layer ($\mathbf{V^1}$)	0.115
Type R lamellae layer ($\mathbf{V^2}$)	0.606
Type C lamellae layer ($\mathbf{V^3}$)	0.279
Lacunar porosity ($\boldsymbol{p_{lac}}$)	0.0082
Newly formed osteons ($\boldsymbol{\phi_a}$)	0.086
Vascular porosity ($\boldsymbol{p_{vas}}$)	0.04

III RESULTS AND DISCUSSION

This work aims to propose a multiscale model of cortical bone by including the TC at the molecular scale. The main objective is to investigate the effect of the principal age-related structural alterations within the TC, namely the change in the diameter (due to change in the molecule degree of hydration) and the change in the number of H-bonds, on bone mechanical properties at different hierarchical levels.

In this section, we first present and discuss the results of our proposed model at different scales, with the TC-related inputs corresponding to the ideal case in healthy mature cortical bone ($N = 30$ and $D_{TC} = 1.5\,nm$). In order to validate our approach, we compare the obtained results with experimental data and multiscale model results available in the literature. Then, we examine the effect of the H-bond number and the TC diameter on bone mechanical behavior at different levels of its hierarchical structure. We focus on the effect of each parameter acting alone. More attention is devoted to the upper scales since the effect of these two parameters on the TC mechanical behavior at the molecular scale has been previously presented and discussed in (Mouss et al., 2020).

It should be noted that the proposed model was tested with a well-defined configuration, as described in *section II*. Studies of the variation of mechanical and geometrical parameters, of different bone constituents' volume fractions, or the variation of bone porosity on the macroscopic mechanical properties of the cortical bone are beyond the scope of the present paper. These studies have already been performed by previous bone multiscale modeling studies published in the literature (Barkaoui et al., 2014; Fritsch and Hellmich, 2007; Hamed et al., 2010; Martínez-Reina et al., 2011).

III.1 Model validation

The TC effective Young's modulus (E_{app}=4.41GPa) predicted using the proposed FE model in the ideal case ($N = 30$ and $D_{TC} = 1.5\,nm$) is in good agreement with earlier values published in the literature. It is within the range of available experimental results (between 0.35 and 12.2 GPa) and is consistent with computational studies, particularly with the results reported in (Lorenzo and Caffarena, 2005) and (Gautieri et al., 2008) (4.8 GPa and 4.56 GPa, respectively) (**Table 4**). Moreover, the FE result is in agreement with the SMD study demonstrating that the Young's modulus of TC molecules is rate-dependent tending towards to 4GPa under loading rates slower than 0.5m/s (Gautieri et al., 2009).

Table 4: Comparison between experimental and numerical approaches for estimating the Young's modulus of a single tropocollagen molecule.

Young's modulus (GPa)	Method	Reference
≈9	Brillouin light scattering (Rat tail tendon)	(Harley et al., 1977)
≈5.1	Brillouin light scattering (Rat tail tendon)	(Cusack and Miller, 1979)
3–5.1	Electron microscopy (Calf skin)	(Hofmann et al., 1984)
2.9±0.1	X-ray diffraction (Bovine Achilles tendon)	(Sasaki and Odajima, 1996)
0.35–12	Optical tweezer (Human pro-collagen)	(Sun et al., 2002)
4.1	MLR (Lathyritic rat skin)	(Nestler et al., 1983)
≈7	Reactive atomistic modeling	(Buehler, 2006)
4.59±0.38	Atomistic modeling	(Gautieri et al., 2008)
≈4	Atomistic modeling	(Gautieri et al., 2009)
4.41	**Finite element model**	**Present work**

The observed variability of the Young's modulus of the TC reported in the literature can be explained by several factors. With experimental techniques, it may be related to the difference in the properties of the experimented collagen in different tissues (**Table 4**). This hypothesis is supported by instances that revealed that the Young's modulus of collagen reconstituted from calf skin is larger than that of collagen reconstituted from bovine tendon by an order of magnitude (Sasaki and Odajima, 1996).

The differences between Young's modulus values using MD simulation studies is probably due to differences in the atomistic model. In fact, SMD simulations on TC molecules have been performed with different amino acid sequences in the alpha-chains. (Lorenzo and Caffarena, 2005) who found a value of 4.8 GPa, used a sequence $(\mathrm{Pro}-\mathrm{Hyp}-\mathrm{Gly})_4-\mathrm{Pro}-\mathrm{Hyp}-$ la $-(\mathrm{Pro}-\mathrm{Hyp}-\mathrm{Gly})_5$ while (Buehler, 2006) used a TC sequence of $(\mathrm{Pro}-\mathrm{Hyp}-\mathrm{Gly})_4-\mathrm{Glu}-\mathrm{Lys}-\mathrm{Gly}-(\mathrm{Pro}-\mathrm{Hyp}-\mathrm{Gly})_5$ and assessed the Young's modulus of single TC molecules ranging from 6.99 to 18.82 GPa for various deformation rates. This theory is supported by (Vesentini et al., 2005) and (Gautieri et al., 2008). The former studied the elastic properties of four different type I collagen 30-residue sequences and reported Young's moduli values varying between 1.33 and 2.41 GPa, while the latter tested different amino acid sequences directly and showed that a difference of 30% in elastic modulus may occur.

Table 5 shows the longitudinal elastic moduli of mineralized fibril and fiber, lamellar tissue, single osteon, and cortical bone obtained using our model. This table also gives experimental data available in the literature and the results of the main previously published multi-scale models. It should be noted that the model provides the elastic properties in the three directions after each of the steps described in *section II*. The set of stiffness matrices for all scales of the model is given in *Appendix D*. For comparison purposes, only the longitudinal elastic moduli at the bone scales shown in **Table 5** are presented.

It can be seen that our results are globally within the range of the reported values of elastic moduli from experimental studies. We can also observe a discrepancy in these experimental measurements, specifically at the scale of nanostructures (fibrils and mineralized collagen fibers). This difference can be explained by several factors, including the sample nature. Indeed, Yang and colleagues (Yang et al., 2007), using atomic force microscopy (AFM), tested both native collagen fibrils and cross-linked collagen fibrils, which are thinner than the former ones. The authors reported a longitudinal Young's modulus of approximately 5.4 GPa for the first type of fibrils and 14.7 GPa for the second one. Furthermore, for two collagen fiber samples of the same type (cross-linked) with different hydration states, Law et al. (Law et al., 1989) found that the longitudinal elastic modulus of the wet fiber is more than ten times lower than that of the dry collagen. This remarkable difference in elastic modulus between dry and wet samples was also observed at both levels of the collagen fibrils (Grant et al., 2008; Van Der Rijt et al., 2006) and the osteons (Ascenzi and Bonucci, 1967) (**Table 5**). In addition, the deformation regime also seems to be relevant in the analysis of nanoscale results since, for the same wet fibrils sample, (Eppell et al., 2006) measured a longitudinal Young's modulus of 0.4 GPa and 6 GPa in the small and large-deformations regimen, respectively.

Table 5: Comparison of results from the present model to experimental data and results available in the literature.

Level	Longitudinal elastic modulus (GPa)		
	This model	**Experimental data**	**Multiscale Models**
Nanostructural			
Fibril	$\mathbf{12.13}$	$\mathbf{0.4 - 6}$ (Eppell et al., 2006)	$\mathbf{15.82}$ (Hamed et al., 2010)
		$\mathbf{5 \pm 1}$ (Wenger et al., 2007) $\mathbf{11.5 \pm 2.3}$ (Wenger et al., 2007)	$\mathbf{7.7}$ (Yoon and Cowin, 2008b)
		$\mathbf{5.4 \pm 1.2}$ (Yang et al., 2007) ***(native collagen)*** $\mathbf{14.7 \pm 2.7}$ (Yang et al., 2007) ***(cross-linked collagen)***	$\mathbf{0.935}$ (Barkaoui et al., 2014)
Fiber	$\mathbf{23.89}$	$\mathbf{0.23 \pm 0.04}$ (Law et al., 1989) ***(wet)*** $\mathbf{3.71 \pm 0.67}$ (Law et al., 1989) ***(dry)***	$\mathbf{16.9}$ (Yoon and Cowin, 2008b)
		$\mathbf{6.43 \pm 0,85}$ (Silver et al., 2000)	$\mathbf{12.6}$ (Barkaoui et al., 2014)
Microstructural			
Lamella	$\mathbf{25.38}$	$\mathbf{19.1 \pm 5.4}$ (Zysset et al., 1999)	$\mathbf{24.75}$ (Hamed et al., 2010)
		$\mathbf{21.8 \pm 2.1}$ (Rho et al., 2002)	$\mathbf{22.8}$ (Yoon and Cowin, 2008b)
		$\mathbf{25.1 \pm 2.1}$ (Fan et al., 2002)	$\mathbf{27.6}$ (Barkaoui et al., 2014)
Mesostructural			
Osteon	$\mathbf{24.11}$	$\mathbf{23.4 \pm 6.9}$ (Ascenzi and Bonucci, 1967) ***(dry)***	$\mathbf{17.23}$ (Hamed et al., 2010)
		$\mathbf{11.7 \pm 5.6}$ (Ascenzi and Bonucci, 1967) ***(wet)***	$\mathbf{20.3}$ (Yoon and Cowin, 2008a)
		$\mathbf{22.4 \pm 1.2}$ (Rho et al., 1999)	$\mathbf{29.7}$ (Barkaoui et al., 2014)
Cortical bone	$\mathbf{23.14}$	$\mathbf{17.9 \pm 3.92}$ (Reilly and Burstein, 1975)	$\mathbf{18.69}$ (Hamed et al., 2010)
		$\mathbf{27.4 \pm 0.98}$ (Yoon and Katz, 1976)	$\mathbf{19.5}$ (Martínez-Reina et al., 2011)
		$\mathbf{23.45 \pm 0.21}$ (Turner et al., 1999)	$\mathbf{19.4}$ (Barkaoui et al., 2014)

As compared to the results reported by multi-scale models in the literature, our results seem to be slightly higher. Then again, differences between model values can be noticed (**Table 5**). These differences can be explained firstly by the authors' choice of mechanical properties and volume fractions of bone constituents in their multiscale model. Indeed, there is a wide range of values in the literature for the elastic moduli of collagen and mineral crystals, whereas fewer data are available for the mechanical properties of NPCs. Different choices for these properties can lead to significantly different results. In our model, for example, the fitted analytical equation derived from the parametric study estimates the Young's modulus of the ideal collagen to be approximately 4.41 GPa, which is higher than the input values used by (Yoon and Cowin, 2008a, 2008b) and (Barkaoui et al., 2014) (1.2 GPa and 2.5 GPa, respectively). Regarding the Young's modulus of the hydroxyapatite crystals, we selected the value 114 GPa similarly to (Yoon and Cowin, 2008a, 2008b), while both (Barkaoui et al., 2014) and (Hamed et al., 2010) used 120 GPa. On the other hand, the mineral volume fraction is crucial in the mechanical behavior modeling of bone tissue since the variation of this parameter can explain certain physiological phenomena, such as the differences between young and mature bone or between healthy and diseased bone (osteoporotic bone, for example). The way this volume fraction was estimated differs from one multiscale model to another. For instance, (Yoon and Cowin, 2008a, 2008b) considered that the intrafibrillar mineral represents 25% of the total mineral content and simply assume that the rest is equally shared (37.5% and 37.5%) between the interfibrillar and the interlamellar space. Furthermore, these ratios were fixed, as the authors did not consider any variation in the mineral content. In contrast, in our model, the mineral distribution of reference bone minerals was assumed to be equal to 28, 58, and 14% for the intra-fibrillar, inter-fibrillar, and inter-lamellar spaces, respectively (Martínez-Reina et al., 2011; ROBINSON and ELLIOTT, 1957). The intra-fibrillar fraction is similar, but the other fractions are different from the values assumed by (Yoon and Cowin, 2008a, 2008b). In this regard, the 58% volume fraction of the inter-fibrillar mineral in our model may have significantly contributed to the abrupt increase in longitudinal Young's modulus at the collagen fiber scale (**Table 5**).

Second, there are differences between the models with regard to the method of estimating mechanical properties at some scales. As an example, to estimate the mechanical properties of the extra-fibrillar mineral where fibrils are unidirectionally embedded to form a mineralized collagen fiber, we used the Mori-Tanaka homogenization method. The advantage of this

approach is that it takes fibril interactions into consideration. In their work, (Hamed et al., 2010) also applied this method to estimate the effective properties of bone at this level, whereas (Yoon and Cowin, 2008a, 2008b) and (Barkaoui et al., 2014) used the bounds of Reus and Voigt. As another example, starting from the lamellar scale, the estimation of the isotropic transverse elastic properties of the osteon in our model was performed in several steps considering the different types of porosities (canaliculi and lacunae) as well as their different orientations. This method, based on the work of (Yoon and Cowin, 2008a, 2008b), was also used by (Martínez-Reina et al., 2011) and (Barkaoui et al., 2014), while (Hamed et al., 2010) used the formulation of (Sun and Li, 1988) for laminated composites.

Finally, the way in which the scales are defined in our model is not unique or fixed. While there is a consensus regarding the classification of the principal scales, some dissimilarity regarding the intermediate levels exists. For example, (Hamed et al., 2010) considered only four hierarchical levels, namely the mineralized collagen fibril, the single lamella, the single osteon, and the cortical bone scale. In turn, (Barkaoui et al., 2014) considered the microfibrils as substructures of collagen fibrils and consequently defined one more scale. According to the authors, the consideration of this fibril substructure scale explains their low predicted value for the longitudinal elastic modulus of the fibril, as compared to the other multiscale models (**Table 5**).

It should be noted that the osteon-scale mechanical properties reported in **Table 5** refer specifically to type L osteons, those having collagen fibers aligned with the longitudinal axis (**Figure 8**). Except for the model proposed by (Yoon and Cowin, 2008a, 2008b), the existing models in the literature only consider type L osteons. In our case, we were also interested in estimating the mechanical properties of the other two types of osteons (type T and A), by rotating the orientation of the collagen fibers using simple tensorial transformation laws at Step 4 as described in section II. The obtained stiffness matrices are presented in *Appendix D*. They are qualitatively in good agreement with the results obtained from (Yoon and Cowin, 2008a, 2008b): type T osteon is more rigid along the transverse direction ($E_2 > E_3 > E_1$), while type A osteon is more rigid along both the longitudinal and transverse directions ($E_2 = E_3 > E_1$).

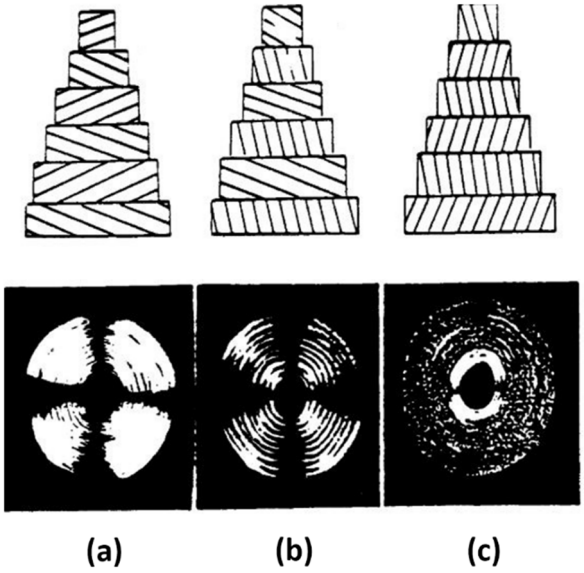

Figure 8: Different types of osteons: T (a), A (b) and L (c).

After testing the proposed multiscale model for cortical bone in the case of the ideal collagen molecule, we investigated the model response in different situations by varying the input values related to the TC: the number of intramolecular bonds and the degree of hydration (represented by the molecular diameter). The objective was to assess the effect of structural alterations occurring at the level of these two molecular-scale parameters on the mechanical properties of the upper hierarchical bone scales. **Figure 9** summarizes the results of our investigations.

III.2 Effect of H-bonds

It can be clearly observed that the deterioration of the H-bonds within the TC leads to a decrease in the longitudinal elastic modulus at all scales, for all values of the molecular diameter. In the specific case of the TC at the molecular scale, the significant decrease in the TC effective Young's modulus occurring with a decrease in the number of H-bonds was also observed by (Gautieri et al., 2008) using SMD simulations. This loss in stiffness becomes less significant when transitioning from one scale to the upper scale, however. In the case of a wet TC, for example, considering the intermediate scale of the lamella, the longitudinal elastic modulus decreases by 14% when N drops from 30 to 0, against a decrease of 16% and 12% at the fiber and osteon scales, respectively.

On the other hand, for each hierarchical level, the elastic modulus decrease is more pronounced for the largest diameters. For example, the elastic modulus of the fibril decreases by 15% when the number of H-bonds (N) drops from 30 to 0 in the case of dry TC ($D_{TC} =$

$1\ nm$), while it decreases by 42% and 54% in the case of semi-wet ($D_{TC} = 1.23\ nm$) and wet ($D_{TC} = 1.5\ nm$) TC, respectively. Note that although the case of unbound polypeptide chains (N=0) is unrealistic and biologically irrelevant, it still allowed us to qualitatively and quantitatively describe the contribution of H-bonds to the bone strength at different scales.

In conclusion, this study highlights the significant contribution of the H-bonds linking the polypeptide chains within the TC triple-helix structure to the mechanical properties of bone at different hierarchical scales. Several experimental and numerical studies have investigated the effect of cross-links between collagen molecules on the mechanical behavior of bone (Barkaoui and Hambli, 2014; Buehler, 2008; Campagnola and Loew, 2003; Depalle et al., 2015; Saito and Marumo, 2010; Viguet-Carrin et al., 2006). However, to the best of our knowledge, the influence of H-bonds within these molecules on upper scales of bone has not been addressed yet, which does not allow us to compare our results so far.

III.3 Effect of the degree of hydration of tropocollagen (phase II)

The TC dehydration also seems to affect the elastic properties at the different hierarchical levels but in a less pronounced way in comparison with the effect of a loss of H-bonds. In fact, for a given number of H-bonds, the decrease in TC diameter induces an increase in longitudinal elastic modulus for all the bone scales (**Figure 9**). The most relevant increase is observed at the fibril scale and is 15.5% for N=0 when changing from a wet TC ($D_{TC} = 1.5\ nm$) to a dry case ($D_{TC} = 1\ nm$). Under these same conditions at higher hierarchical levels (mineralized collagen fiber scale and upper scales), we observe almost the same increase rate below 4.2%. Furthermore, it can be noticed that for all scales, TC dehydration has a weak effect with large numbers of H-bonds, but this effect becomes more pronounced as the number of H-bonds decreases. For example, at the collagen fiber scale, the transition from wet ($D_{TC} = 1.5\ nm$) to dry ($D_{TC} = 1\ nm$) TC leads to a 4.6% increase in the longitudinal elastic modulus when N=30, while an increase of 14% is observed for N=12. In the particular case where N=30, a negligible effect (<0.1%) is noted for all scales when transiting from a semi-wet ($D_{TC} = 1.23\ nm$) to a wet TC ($D_{TC} = 1\ nm$).

In a multiscale study evaluating the effect of collagen mechanical properties on the overall mechanical properties of cortical bone, (Hamed et al., 2010) tested a higher value for the elastic modulus corresponding to dry collagen (5.4 GPa) instead of the modulus initially used in their multiscale model (2.5 GPa). The authors found that this 116% increase in the Young's modulus of collagen resulted in a 39.8 and 35.9% increase in the longitudinal and

transverse moduli of bone elasticity, respectively. These results are qualitatively consistent with the results of our model. Indeed, in our case, starting from an initial value of 4.41 GPa of the elastic modulus of wet collagen, dehydration of the TC caused an increase of 28% in the apparent Young's modulus of the molecule leading to about a 4% increase in the longitudinal elastic modulus of the cortical bone.

Such an increase in the elastic modulus upon dehydration has been widely demonstrated by previous experimental studies at different scales of the hierarchical structure of bone: at the organ level (trabecular bone and cortical bone) (Broz et al., 1993; Frank et al., 2018; Nyman et al., 2013; Nyman et al., 2006; Sedlin and Hirsch, 1966; Smith and Walmsley, 1959; Townsend et al., 1975; Wolfram et al., 2010; Yan et al., 2008), at the tissue level (lamellae and osteons) (Hengsberger et al., 2002; Rho and Pharr, 1999), and the ultrastructural levels (microfibrils, fibrils, and collagen fiber) (Eppell et al., 2006; Fielder and Nair, 2019; Shen et al., 2008; Van Der Rijt et al., 2006; Wenger et al., 2007; Zhang et al., 2007). Numerical studies based on the FE method and molecular dynamics mainly focusing on nanoscale structures, have also investigated the effect of water on the mechanical properties of bone and reached the same conclusion (Fielder and Nair, 2019; Gautieri et al., 2011; Hambli and Barkaoui, 2012; Mouss et al., 2020; Siegmund et al., 2008; Yuan et al., 2011). In addition, some of these studies showed that dehydration of bone compromised its quality by making it stiffer and stronger, but brittle, with almost no plastic deformation before failure (Broz et al., 1993; Currey, 1988; Dempster and Liddicoat, 1952; Nomura et al., 1977; Sedlin and Hirsch, 1966; Smith and Walmsley, 1959; Townsend et al., 1975; Weiner and Wagner, 1998). Given these findings, some researchers have recently suggested that the amount of water in bone could potentially be used as a meaningful index in assessing patients' risk of fragility (Samuel et al., 2016; Unal and Akkus, 2015; Unal et al., 2014). Nevertheless, it is not appropriate to compare our results with the data from these studies, since our study focused only on the effect of water within the TC. The investigation of the effect of dehydration on the mechanical properties of higher scales requires consideration of water outside the collagen molecule as well, such as the water that occupies the void space of the vascular network (Sasaki and Enyo, 1995), the water that resides on the surface of hydroxyapatite (HA) mineral crystals (Jaeger et al., 2005), and the water confined within interstitial nanopores of the extracellular matrix (Pham et al., 2015) or even the water enclosed within the reticular structure of the mineral phase (Maghsoudi-Ganjeh et al., 2020).

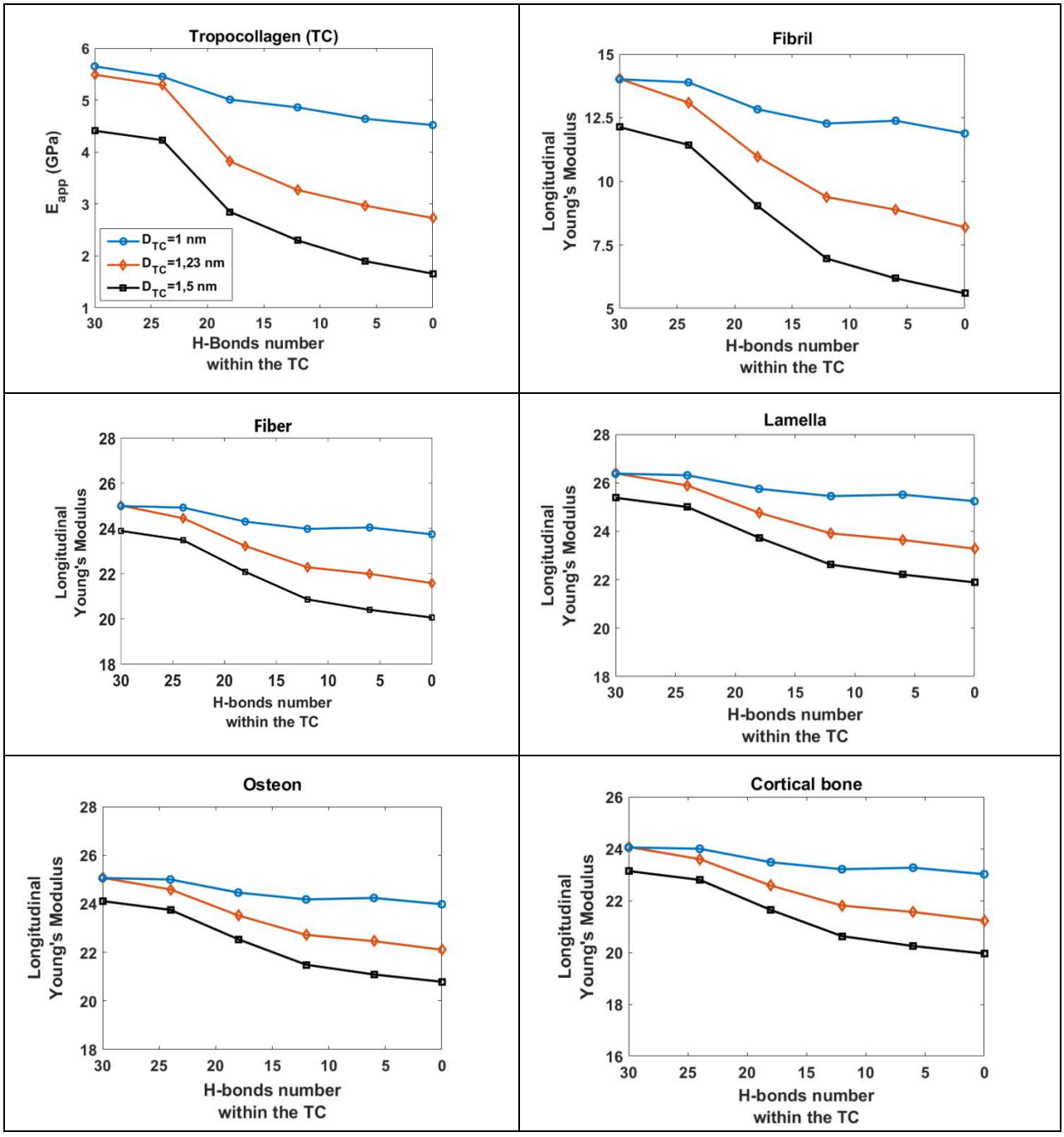

Figure 9: Evolution of the longitudinal Young's modulus at different scales of bone as a function of the number of H-bonds within tropocollagen (TC) and its molecular diameter (D_{TC}).

IV CONCLUSION

In summary, we have proposed a multiscale model to describe the mechanical behavior of cortical bone (a heterogeneous material with a complex structure), by combining the FE method and different analytical homogenization methods. The main assumption of our approach, which differentiates it from previously published multiscale models, is the introduction of the TC, as the lowest hierarchical scale of the bone. To do so, we used the finite element method, but alternative approaches such as the recently proposed atom-to-beam homogenization strategy could also be performed to incorporate this macromolecule into a multiscale model (Kalliauer et al., 2020). The objective was to include the effect of molecular phenomena on the mechanical properties of bone tissue at the macroscopic scale, in particular the structural changes due to aging, namely the decrease in the number of H-bonds within the TC and the dehydration of this molecule.

The results presented demonstrate that the model is able to provide realistic estimates of the elastic properties of bone at different scales in healthy cortical bone (ideal collagen). In addition, they contribute to understanding the contribution of the H-bonds within the collagen molecule and its degree of hydration to the mechanical behavior of the bone at different hierarchical levels, which is not necessarily accessible with current experimental devices.

Among the main limitations of the proposed model is the non-consideration of water-mediated H-bonding at the molecular scale level. Although the TC hydration was related to the molecular diameter, future work could explicitly take this factor into account, which would allow further investigation of the influence of the collagen hydration state on bone mechanical properties. Other limitations can also be mentioned, such as the non-consideration of the interphase layer between collagen and HA crystals, and the effects of cement lines, which make multi-scale modeling of cortical bone a rich and complex problem with much potential for future work.

In future developments, we plan to introduce the effects of aging on the input parameters at different scales and to extend our model by coupling it to a dynamic mathematical bone remodeling model in order to capture the elastic behavior of cortical bone in osteoporosis disease.

ACKNOWLEDGMENT

The authors acknowledge the financial support provided by the Fondation pour la Recherche Médicale (FRM) (Project: DIC20161236439)

CONFLICT OF INTEREST

The authors have no conflict of interest to declare.

APPENDIX A: List of symbols

Symbol	Description
E_{app}	: The apparent Young's modulus of the tropocollagen, defined in **Eq.14**
$\mathbf{C}_{wcol}$	: The effective stiffness tensor of the collagen-water composite, defined in **Eq.15**
$\mathbf{C}_{TC}$	: The stiffness tensors of collagen, defined in **Eq.16**
$\mathbf{C}_{w}$	: The stiffness tensors of water-NPCs, defined in **Eq.17**
$\mathbf{C}_{f}$	: the effective stiffness tensor of the mineralized collagen fibril, defined in **Eq.18**
$\mathbf{C}_{ha}$	: The stiffness tensor of the intrafibrillar mineral, defined in **Eq.19**
$\mathbf{C}_{wha}$	: The stiffness matrix of the extra-fibrillar mineral HA, defined in **Eq.20**
$\mathbf{C}_{F}$	: The effective stiffness tensor of the fiber, defined in **Eq.21**
$\mathbf{C}_{l}$	: The effective stiffness tensor of the lamella, defined in **Eq.22**
$\mathbf{C}_{can}$	: The stiffness tensor of a lamella with canaliculi, defined in **Eq.23**
$\mathbf{C}_{LRC}$	: The effective stiffness tensor of a laminate, defined in **Eq.24**
$\mathbf{C}_{lac}$	: The stiffness tensor of the lamellae with lacunae, defined in **Eq.25**
$\mathbf{C}_{SCS}$	: The stiffness tensor of the secondary lamellar tissue, introduced in **Eq.26**
$\mathbf{C}_{TrI}$	: The effective symmetrized stiffness tensor of the osteon, defined in **Eq.27**
$\mathbf{C}_{TrI}^{a}$	: The stiffness tensor of newly formed osteons, introduced in **Eq.28**
$\mathbf{C}_{TrI}^{b}$	: The stiffness tensor of mature osteons, introduced in **Eq.29**
$\mathbf{C}_{d}$	: The stiffness tensor of the cortical tissue, defined in **Eq.30**
$\mathbf{A}$	: The strain concentration tensor, defined in **Eq.31**
$\mathbf{I}$	: The identity tensor
$\mathbf{S}_{ell}$	: The Eshelby tensor for an ellipsoidal inclusion, introduced in **Eq.32**
$\mathbf{S}_{sph}$	: The Eshelby tensor for a spherical inclusion, introduced in **Eq.33**
$\mathbf{S}_{cyl}$	: The Eshelby tensor for cylindrical inclusion, introduced in **Eq.34**
$\mathbb{P}_{cyl}$	: The Hill polarization tensor for cylindrical inclusions, introduced in **Eq.35**
$\mathbf{P}_{p,wcol}$	: The periodic tensorial operator for platelet-shaped inclusions of mineral crystals in a *cross-linked* collagen matrix, introduced in **Eq.36**
$\mathbf{P}_{c,wha}$	: The periodic tensorial operator for infinite cylindrical periodic inclusions of fibrils embedded in an extra-fibrillar mineral matrix, introduced in **Eq.37**
$\mathbf{P}_{c,l}$	: The periodic operator for infinite cylindrical inclusions in a matrix of lamellar tissue, introduced in **Eq.38**
$\mathbf{P}_{e,LRC}$	: The periodic operator for ellipsoidal inclusions in a matrix of laminate LRC, introduced in **Eq.39**
D_{TC}	: The external diameter of the collagen molecule
N	: The hydrogen bond number within the collagen molecule
A_{TC}	: The equivalent cross-sectional area of a collagen molecule
d_0	: The initial undeformed length of the collagen molecule, introduced in **Eq.40**
F	: The magnitude of stretching load, introduced in **Eq.41**
f	: The nonlinear estimated analytical function linking the apparent Young's modulus of the collagen molecule to its degree of hydration and H-bond number, defined in **Eq.42**
$\{\alpha, \beta, \gamma, \xi\}$	: The regression coefficients of the polynomial approximation, defined in **Eq.43**
ε	: The error of the polynomial approximation, defined in **Eq.44**
ϕ_w	: The volume fraction of water and NPCs within the cross-linked collagen, introduced in **Eq.45**
ϕ_{ha}	: The volume fraction of the intrafibrillar mineral, introduced in **Eq.46**
ϕ_w'	: The volume fraction of the extra-fibrillar water and NPCs, introduced in **Eq.47**
ϕ_f	: The volumetric fraction of fibrils within the fiber, introduced in **Eq.48**
ϕ_F	: The volumetric fraction of fibers within the lamella, introduced in **Eq.49**

ϕ_a : The volume fraction of newly formed osteons, introduced in **Eq.50**

p_{can} : The canalicular porosity, introduced in **Eq.51**

p_{lac} : The lacunar porosity, introduced in **Eq.52**

p_{vas} : The vascular porosity (Haversian canals) , introduced in **Eq.53**

$\mathbf{V}^1$: The volume fraction of the Type L lamellae layer, introduced in **Eq.54**

$\mathbf{V}^2$: The volume fraction of the Type R lamellae layer, introduced in **Eq.55**

$\mathbf{V}^3$: The volume fraction of the Type C lamellae layer, introduced in **Eq.56**

APPENDIX B: Eshelby Tensor

Elliptical inclusion

For the isotropic medium, the Eshelby tensor can be expressed in terms of elliptic integrals (Weinberger and Cai, 2004). Assuming that $a > b > c$ and that the semi-axis a is aligned with the coordinate x (and similarly b with y and c with z) then:

$$\mathcal{S}_{1111} = \frac{3}{8\pi(1-\nu)}a^2 I_{11} + \frac{1-2\nu}{8\pi(1-\nu)}I_1$$

$$\mathcal{S}_{1122} = \frac{1}{8\pi(1-\nu)}b^2 I_{12} + \frac{1-2\nu}{8\pi(1-\nu)}I_1$$

$$\mathcal{S}_{1133} = \frac{1}{8\pi(1-\nu)}c^2 I_{13} + \frac{1-2\nu}{8\pi(1-\nu)}I_1$$

$$\mathcal{S}_{1212} = \frac{a^2 + b^2}{16\pi(1-\nu)}I_{12} + \frac{1-2\nu}{16\pi(1-\nu)}(I_1 + I_2)$$

$$\mathcal{S}_{1112} = \mathcal{S}_{1223} = \mathcal{S}_{1232} = 0$$

where a, b and c specify the size of the ellipsoid and ν is the Poisson coefficient. The other non-zero terms can be found by cyclic permutation ($a \rightarrow b \rightarrow c$ with $1 \rightarrow 2 \rightarrow 3$) of the above formulas. The I terms are defined in terms of standard elliptic integrals (Weinberger and Cai, 2004):

$$I_1 = \frac{4\pi abc}{(a^2-b^2)(a^2-c^2)^{1/2}}[F(\theta,k) - E(\theta,k)]$$

$$I_3 = \frac{4\pi abc}{(b^2-c^2)(a^2-c^2)^{1/2}}\left[\frac{b(a^2-c^2)^{1/2}}{ac} - E(\theta,k)\right]$$

where:

$$\theta = \arcsin\sqrt{\frac{a^2-c^2}{a^2}}$$

$$k = \sqrt{\frac{a^2-b^2}{a^2-c^2}}$$

and:

$$I_1 + I_2 + I_3 = 4\pi$$

$$3I_{11} + I_{12} + I_{13} = \frac{4\pi}{a^2}$$

$$3a^2 I_{11} + b^2 I_{12} + c^2 I_{13} = 3I_1$$

$$I_{12} = \frac{I_2 - I_1}{a^2 - b^2}$$

and the standard elliptic integrals are defined as:

$$F(\theta,k)=\int_0^{\theta}\frac{d\omega}{(1-k^2sin^2\omega)^{1/2}}$$

$$E(\theta,k)=\int_0^{\theta}(1-k^2sin^2\omega)^{1/2}\,d\omega$$

Spherical inclusion

For a spherical inclusion $(a=b=c)$the Eshelby tensor has the following compact expression:

$$\mathcal{S}_{ijkl}=\frac{5\nu-1}{15(1-\nu)}\delta_{ij}\delta_{kl}+\frac{4-5\nu}{15(1-\nu)}(\delta_{ik}\delta_{jl}+\delta_{il}\delta_{jk})$$

where $\delta_{ij}$is the Kronecker delta. One can notice that the tensor itself does not depend on the radius of the sphere.

Cylindrical inclusion

For an elliptical cylinder ($c\rightarrow\infty$) :

$$\mathcal{S}_{1111}=\frac{1}{2(1-\nu)}\left[\frac{b^2+2ab}{(a+b)^2}+(1-2\nu)\frac{b}{a+b}\right]$$

$$\mathcal{S}_{2222}=\frac{1}{2(1-\nu)}\left[\frac{a^2+2ab}{(a+b)^2}+(1-2\nu)\frac{a}{a+b}\right]$$

$$\mathcal{S}_{3333}=0$$

$$\mathcal{S}_{1122}=\frac{1}{2(1-\nu)}\left[\frac{b^2}{(a+b)^2}-(1-2\nu)\frac{b}{a+b}\right]$$

$$\mathcal{S}_{2233}=\frac{1}{2(1-\nu)}\frac{2\nu a}{a+b}$$

$$\mathcal{S}_{2211}=\frac{1}{2(1-\nu)}\left[\frac{a^2}{(a+b)^2}-(1-2\nu)\frac{a}{a+b}\right]$$

$$\mathcal{S}_{3311}=\mathcal{S}_{3322}=0$$

$$\mathcal{S}_{1111}=\frac{1}{2(1-\nu)}\left[\frac{a^2+b^2}{2(a+b)^2}+\frac{(1-2\nu)}{2}\right]$$

$$\mathcal{S}_{1133}=\frac{1}{2(1-\nu)}\frac{2\nu b}{a+b}$$

$$\mathcal{S}_{1133}=\frac{a}{2(a+b)}\qquad\mathcal{S}_{1133}=\frac{b}{2(a+b)}$$

APPENDIX C: Periodic Operator Tensor

The fourth-order tensor of the periodic operator for isotropic materials is given by (Nemat-Nasser and Hori, 2013) as follows:

$$P = \sum_{\xi}{}' \phi\, g(-\xi)\, g(\xi)\, FP(\xi)$$

where the apostrophe on the sum indicates that $\xi = 0$ is excluded. $g(\xi)$ is called the g-integral function and represents the geometry of a cavity. It is defined as the volume integral of $exp(i\xi.x)$ on this cavity. The variable ξ is given by $\xi \equiv \frac{n_i \pi}{a_i}$where n_i is the number of unit cells in the direction i. Note that i can be replaced by x, y, z for the directions x, y and z respectively and that the domain of a unit cell is given by $U = \{x;\ -a_i < x_i < a_i\ (i = x, y, z)\}$. The fourth order tensor $FP(\xi)$ for anisotropic symmetry is defined in the work of (Nemat-Nasser and Hori, 2013) as :

$$FP(\xi) = sym\,\{\xi \otimes (\xi.C.\xi)^{-1} \otimes \xi\} : C$$

where C is the fourth rank elasticity tensor of the bone matrix and the term $(\xi.C.\xi)$ can be expressed using index notation as follows:

$$\begin{aligned}\left(\xi_i C_{ijkl} \xi_l\right) = {} & \xi_1 C_{1jk1} \xi_1 + \xi_1 C_{1jk2} \xi_2 + \xi_1 C_{1jk3} \xi_3 \\ & + \xi_2 C_{2jk1} \xi_1 + \xi_2 C_{2jk2} \xi_2 + \xi_2 C_{2jk3} \xi_3 \\ & + \xi_3 C_{3jk1} \xi_1 + \xi_3 C_{3jk2} \xi_2 + \xi_3 C_{3jk3} \xi_3\end{aligned}$$

Note that the summation in the previous equation with respect to ξ (or n_x, n_y and n_z) is generally 1 at infinity. Nevertheless, in our case the summation has been performed from 1 to $\pm$ 50 since (Nemat-Nasser and Hori, 2013) have shown that the summation up to $\pm$ 40 is only 0.7% less precise than the summation up to $\pm$ 50.

As previously mentioned, the g-integral function is calculated as a function of the shape of the inclusion. Three shapes of inclusions were used in the model: cubic (for mineral crystals), infinite cylindrical (for collagen fibers and fibrils) and ellipsoidal (for lacunar porosity). The expression of $g(\xi)$ in each of these cases is given below (Nemat-Nasser et al., 1993):

Ellipsoidal shape

$$g(\xi) = \frac{3}{\eta^3}(\sin\eta - \eta\cos\eta) \qquad (\eta \neq 0)$$

where:

$$\eta = \pi \sqrt{\left(n_x \frac{b_x}{a_x}\right)^2 + \left(n_y \frac{b_y}{a_y}\right)^2 + \left(n_z \frac{b_z}{a_z}\right)^2}$$

x, y and z indicate three perpendicular directions. The number of cavities in the directions x, y and z directions is indicated by n_x, n_y and n_z. The lengths of the principal axes of an ellipsoidal shape representing a gap are denoted by b_x, b_y and b_z. For the L-type osteon, the approximate dimensions of a lacuna are $b_x = 5\mu m$, $b_y = 10\mu m$, and $b_z = 25\mu m$.

Cylindrical shape

$$g(\xi) = \begin{cases} \frac{2}{B} J_1(B) & si\ nz = 0 \\ 0 & si\ nz \neq 0 \end{cases}$$

where $J1$ is the Bessel function of order 1 and:

$$B = \pi \sqrt{\left(n_x \frac{b_x}{a_x}\right)^2 + \left(n_y \frac{b_y}{a_y}\right)^2}$$

n_x and n_y are the number of cylindrical inclusions in the directions x and y respectively.

Cubic shape

$$g(\xi) = \frac{\sin L_x \sin L_y \sin L_z}{L_x L_y L_z}$$

where $L_i = \xi_i l_i$. The index i is replaced by x, y and z to indicate three perpendicular directions, and l_i is the size of the platelet-shaped mineral crystals ($l_x = 3$nm, $l_y = 25$nm and $l_z = 50$nm).

APPENDIX D: Stiffness Matrices at different hierarchical levels of the multi-scale model of cortical bone (values in GPa)

Cross-linked **collagen:**

$$C_{wcol} = \begin{pmatrix} 5.10 & 2.95 & 2.95 & 0 & 0 & 0 \\ 2.95 & 5.10 & 2.95 & 0 & 0 & 0 \\ 2.95 & 2.95 & 5.94 & 0 & 0 & 0 \\ 0 & 0 & 0 & 2.79 & 0 & 0 \\ 0 & 0 & 0 & 0 & 2.79 & 0 \\ 0 & 0 & 0 & 0 & 0 & 2.58 \end{pmatrix}$$

Mineralized collagen fibril:

$$C_f = \begin{pmatrix} 10.29 & 5.59 & 5.60 & 0 & 0 & 0 \\ 5.59 & 13.29 & 5.99 & 0 & 0 & 0 \\ 5.60 & 5.99 & 16.03 & 0 & 0 & 0 \\ 0 & 0 & 0 & 8.02 & 0 & 0 \\ 0 & 0 & 0 & 0 & 9.97 & 0 \\ 0 & 0 & 0 & 0 & 0 & 7.61 \end{pmatrix}$$

Extrafibrillar mineral:

$$C_{wha} = \begin{pmatrix} 48.78 & 16.86 & 16.86 & 0 & 0 & 0 \\ 16.86 & 48.78 & 16.86 & 0 & 0 & 0 \\ 16.86 & 16.86 & 48.78 & 0 & 0 & 0 \\ 0 & 0 & 0 & 40.07 & 0 & 0 \\ 0 & 0 & 0 & 0 & 40.07 & 0 \\ 0 & 0 & 0 & 0 & 0 & 40.07 \end{pmatrix}$$

Mineralized collagen fiber:

$$C_F = \begin{pmatrix} 25.63 & 10.30 & 10.14 & 0 & 0 & 0 \\ 10.30 & 27.50 & 10.39 & 0 & 0 & 0 \\ 10.14 & 10.39 & 29.61 & 0 & 0 & 0 \\ 0 & 0 & 0 & 21.09 & 0 & 0 \\ 0 & 0 & 0 & 0 & 22.32 & 0 \\ 0 & 0 & 0 & 0 & 0 & 20.91 \end{pmatrix}$$

Lamella:

$$C_l = \begin{pmatrix} 27.14 & 10.92 & 10.62 & 0 & 0 & 0 \\ 10.92 & 28.94 & 10.87 & 0 & 0 & 0 \\ 10.62 & 10.87 & 31.31 & 0 & 0 & 0 \\ 0 & 0 & 0 & 22.58 & 0 & 0 \\ 0 & 0 & 0 & 0 & 23.77 & 0 \\ 0 & 0 & 0 & 0 & 0 & 22.46 \end{pmatrix}$$

Lamella with canaliculus:

$$C_{can} = \begin{pmatrix} 26.01 & 10.47 & 10.18 & 0 & 0 & 0 \\ 10.47 & 27.73 & 10.41 & 0 & 0 & 0 \\ 10.18 & 10.41 & 30.01 & 0 & 0 & 0 \\ 0 & 0 & 0 & 21.63 & 0 & 0 \\ 0 & 0 & 0 & 0 & 22.78 & 0 \\ 0 & 0 & 0 & 0 & 0 & 21.52 \end{pmatrix}$$

Laminate with lamellae LRC:

$$C_{LRC} = \begin{pmatrix} 26.01 & 10.47 & 10.18 & 0 & 0 & 0 \\ 10.47 & 27.73 & 10.41 & 0 & 0 & 0 \\ 10.18 & 10.41 & 30.01 & 0 & 0 & 0 \\ 0 & 0 & 0 & 21.63 & 0 & 0 \\ 0 & 0 & 0 & 0 & 22.78 & 0 \\ 0 & 0 & 0 & 0 & 0 & 21.52 \end{pmatrix}$$

Osteon:

Type of osteon	Orthotropic results	Isotropic-Transverse Results
Type L	$C_{lacL} = \begin{pmatrix} 25.72 & 10.36 & 10.07 & 0 & 0 & 0 \\ 10.36 & 27.46 & 10.31 & 0 & 0 & 0 \\ 10.07 & 10.31 & 29.73 & 0 & 0 & 0 \\ 0 & 0 & 0 & 21.43 & 0 & 0 \\ 0 & 0 & 0 & 0 & 22.57 & 0 \\ 0 & 0 & 0 & 0 & 0 & 21.32 \end{pmatrix}$	$C_{TrIL} = \begin{pmatrix} 27.76 & 9.16 & 10.19 & 0 & 0 & 0 \\ 9.16 & 27.76 & 10.19 & 0 & 0 & 0 \\ 10.19 & 10.19 & 29.73 & 0 & 0 & 0 \\ 0 & 0 & 0 & 21.99 & 0 & 0 \\ 0 & 0 & 0 & 0 & 21.99 & 0 \\ 0 & 0 & 0 & 0 & 0 & 18.59 \end{pmatrix}$
Type T	$C_{lacT} = \begin{pmatrix} 27.76 & 10.07 & 10.36 & 0 & 0 & 0 \\ 10.07 & 29.73 & 10.31 & 0 & 0 & 0 \\ 10.36 & 10.31 & 27.46 & 0 & 0 & 0 \\ 0 & 0 & 0 & 22.57 & 0 & 0 \\ 0 & 0 & 0 & 0 & 21.43 & 0 \\ 0 & 0 & 0 & 0 & 0 & 21.32 \end{pmatrix}$	$C_{TrIT} = \begin{pmatrix} 28.52 & 9.16 & 10.33 & 0 & 0 & 0 \\ 9.16 & 28.52 & 10.33 & 0 & 0 & 0 \\ 10.33 & 10.33 & 27.46 & 0 & 0 & 0 \\ 0 & 0 & 0 & 21.99 & 0 & 0 \\ 0 & 0 & 0 & 0 & 21.99 & 0 \\ 0 & 0 & 0 & 0 & 0 & 19.36 \end{pmatrix}$
Type A	$C_{lacA} = \begin{pmatrix} 26.82 & 10.11 & 10.31 & 0 & 0 & 0 \\ 10.11 & 28.35 & 10.33 & 0 & 0 & 0 \\ 10.31 & 10.33 & 27.72 & 0 & 0 & 0 \\ 0 & 0 & 0 & 22.42 & 0 & 0 \\ 0 & 0 & 0 & 0 & 21.53 & 0 \\ 0 & 0 & 0 & 0 & 0 & 21.35 \end{pmatrix}$	$C_{TrIA} = \begin{pmatrix} 28.49 & 9.18 & 10.32 & 0 & 0 & 0 \\ 9.18 & 28.49 & 10.32 & 0 & 0 & 0 \\ 10.32 & 10.32 & 27.72 & 0 & 0 & 0 \\ 0 & 0 & 0 & 21.97 & 0 & 0 \\ 0 & 0 & 0 & 0 & 21.97 & 0 \\ 0 & 0 & 0 & 0 & 0 & 19.31 \end{pmatrix}$

Cortical bone:

$$C_d = \begin{pmatrix} 26.65 & 8.79 & 9.78 & 0 & 0 & 0 \\ 8.79 & 26.65 & 9.78 & 0 & 0 & 0 \\ 9.78 & 9.78 & 28.54 & 0 & 0 & 0 \\ 0 & 0 & 0 & 20.99 & 0 & 0 \\ 0 & 0 & 0 & 0 & 20.99 & 0 \\ 0 & 0 & 0 & 0 & 0 & 17.85 \end{pmatrix}$$

REFERENCES

Akiva, U., Wagner, H. D., & Weiner, S. (1998). Modelling the three-dimensional elastic constants of parallel-fibred and lamellar bone. *Journal of Materials Science*, *33*(6), 1497-1509.

Akkus, O. (2005). Elastic deformation of mineralized collagen fibrils: an equivalent inclusion based composite model.

Ascenzi, A., & Bonucci, E. (1967). The tensile properties of single osteons. *The Anatomical Record*, *158*(4), 375-386.

Ascenzi, M.-G., Gill, J., & Lomovtsev, A. (2008). Orientation of collagen at the osteocyte lacunae in human secondary osteons. *Journal of biomechanics*, *41*(16), 3426-3435.

Bailey, A. J., Paul, R. G., & Knott, L. (1998). Mechanisms of maturation and ageing of collagen. *Mechanisms of Ageing and Development*, *106*(1), 1-56. https://doi.org/https://doi.org/10.1016/S0047-6374(98)00119-5

Barkaoui, A., Bettamer, A., & Hambli, R. (2011). Failure of mineralized collagen microfibrils using finite element simulation coupled to mechanical quasi-brittle damage. *Procedia Engineering*, *10*, 3185-3190.

Barkaoui, A., Chamekh, A., Merzouki, T., Hambli, R., & Mkaddem, A. (2014). Multiscale approach including microfibril scale to assess elastic constants of cortical bone based on neural network computation and homogenization method. *International journal for numerical methods in biomedical engineering*, *30*(3), 318-338.

Barkaoui, A., & Hambli, R. (2011). Finite element 3D modeling of mechanical behavior of mineralized collagen microfibrils. *Journal of Applied Biomaterials and Biomechanics*, *9*(3), 199-206.

Barkaoui, A., & Hambli, R. (2014). Nanomechanical properties of mineralised collagen microfibrils based on finite elements method: biomechanical role of cross-links. *Computer methods in biomechanics and biomedical engineering*, *17*(14), 1590-1601.

Barkaoui, A., Hambli, R., & Tavares, J. M. R. (2015). Effect of material and structural factors on fracture behaviour of mineralised collagen microfibril using finite element simulation. *Computer methods in biomechanics and biomedical engineering*, *18*(11), 1181-1190.

Barros, E. M. K. P., Rodrigues, C. J., Rodrigues, N. R., Oliveira, R. P., Barros, T. E. P., & Rodrigues, A. J. (2002). Aging of the elastic and collagen fibers in the human cervical interspinous ligaments. *The Spine Journal*, *2*(1), 57-62. https://doi.org/https://doi.org/10.1016/S1529-9430(01)00167-X

Bella, J., Brodsky, B., & Berman, H. M. (1995). Hydration structure of a collagen peptide. *Structure*, *3*(9), 893-906. https://doi.org/https://doi.org/10.1016/S0969-2126(01)00224-6

Bella, J., Eaton, M., Brodsky, B., & Berman, H. M. (1994). Crystal and molecular structure of a collagen-like peptide at 1.9 A resolution [10.1126/science.7695699]. *Science*, *266*(5182), 75.

Beno, T., Yoon, Y.-J., Cowin, S. C., & Fritton, S. P. (2006). Estimation of bone permeability using accurate microstructural measurements. *Journal of biomechanics*, *39*(13), 2378-2387.

Benveniste, Y. (1987). A new approach to the application of Mori-Tanaka's theory in composite materials. *Mechanics of materials*, *6*(2), 147-157.

Bhagavan, N. V. (2001). *Medical Biochemistry*. Elsevier Science.

Bhattacharjee, A., & Bansal, M. (2008). Collagen Structure: The Madras Triple Helix and the Current Scenario. *IUBMB Life*, *57*(3), 161-172. https://doi.org/10.1080/15216540500090710

Brodsky, B., & Ramshaw, J. A. M. (1997). The collagen triple-helix structure. *Matrix Biology*, *15*(8), 545-554. https://doi.org/https://doi.org/10.1016/S0945-053X(97)90030-5

Broz, J., Simske, S., Greenberg, A., & Luttges, M. (1993). Effects of rehydration state on the flexural properties of whole mouse long bones.

Brynk, T., Hellmich, C., Fritsch, A., Zysset, P., & Eberhardsteiner, J. (2011). Experimental poromechanics of trabecular bone strength: role of Terzaghi's effective stress and of tissue level stress fluctuations. *Journal of biomechanics*, *44*(3), 501-508.

Budiansky, B. (1965). On the elastic moduli of some heterogeneous materials. *Journal of the Mechanics and Physics of Solids*, *13*(4), 223-227.
Budyn, E., & Hoc, T. (2010). Analysis of micro fracture in human Haversian cortical bone under transverse tension using extended physical imaging. *International Journal for Numerical Methods in Engineering*, *82*(8), 940-965.
Buehler, M. J. (2006). Atomistic and continuum modeling of mechanical properties of collagen: Elasticity, fracture, and self-assembly. *Journal of Materials Research*, *21*(8), 1947-1961. https://doi.org/10.1557/jmr.2006.0236
Buehler, M. J. (2008). Nanomechanics of collagen fibrils under varying cross-link densities: atomistic and continuum studies. *Journal of the mechanical behavior of biomedical materials*, *1*(1), 59-67.
Buehler, M. J., & Wong, S. Y. (2007). Entropic Elasticity Controls Nanomechanics of Single Tropocollagen Molecules. *Biophysical Journal*, *93*(1), 37-43. https://doi.org/https://doi.org/10.1529/biophysj.106.102616
Campagnola, P. J., & Loew, L. M. (2003). Second-harmonic imaging microscopy for visualizing biomolecular arrays in cells, tissues and organisms. *Nature Biotechnology*, *21*, 1356. https://doi.org/10.1038/nbt894
Charvolin, J., & Sadoc, J.-F. (2012). About collagen, a tribute to Yves Bouligand [10.1098/rsfs.2012.0014]. *Interface Focus*, *2*(5), 567.
Chen, J.-H., Liu, C., You, L., & Simmons, C. A. (2010). Boning up on Wolff's Law: Mechanical regulation of the cells that make and maintain bone. *Journal of Biomechanics*, *43*(1), 108-118. https://doi.org/https://doi.org/10.1016/j.jbiomech.2009.09.016
Chou, P., Carleone, J., & Hsu, C. (1972). Elastic constants of layered media. *Journal of Composite Materials*, *6*(1), 80-93.
Currey, J. D. (1969). The relationship between the stiffness and the mineral content of bone. *Journal of Biomechanics*, *2*(4), 477-480. https://doi.org/https://doi.org/10.1016/0021-9290(69)90023-2
Currey, J. D. (1988). The effects of drying and re-wetting on some mechanical properties of cortical bone. *Journal of biomechanics*, *21*(5), 439-441.
Cusack, S., & Miller, A. (1979). Determination of the elastic constants of collagen by Brillouin light scattering. *Journal of Molecular Biology*, *135*(1), 39-51. https://doi.org/https://doi.org/10.1016/0022-2836(79)90339-5
Dempster, W. T., & Liddicoat, R. T. (1952). Compact bone as a non-isotropic material. *American Journal of Anatomy*, *91*(3), 331-362.
Depalle, B., Qin, Z., Shefelbine, S. J., & Buehler, M. J. (2015). Influence of cross-link structure, density and mechanical properties in the mesoscale deformation mechanisms of collagen fibrils. *Journal of the Mechanical Behavior of Biomedical Materials*, *52*, 1-13. https://doi.org/https://doi.org/10.1016/j.jmbbm.2014.07.008
Eklouh-Molinier, C., Happillon, T., Bouland, N., Fichel, C., Diébold, M.-D., Angiboust, J.-F., . . . Piot, O. (2015). Investigating the relationship between changes in collagen fiber orientation during skin aging and collagen/water interactions by polarized-FTIR microimaging [10.1039/C5AN00278H]. *Analyst*, *140*(18), 6260-6268. https://doi.org/10.1039/C5AN00278H
Eppell, S., Smith, B., Kahn, H., & Ballarini, R. (2006). Nano measurements with micro-devices: mechanical properties of hydrated collagen fibrils. *Journal of the Royal Society Interface*, *3*(6), 117-121.
Fan, Z., Swadener, J., Rho, J., Roy, M., & Pharr, G. (2002). Anisotropic properties of human tibial cortical bone as measured by nanoindentation. *Journal of orthopaedic research*, *20*(4), 806-810.
Fielder, M., & Nair, A. K. (2019). Effects of hydration and mineralization on the deformation mechanisms of collagen fibrils in bone at the nanoscale. *Biomechanics and modeling in mechanobiology*, *18*(1), 57-68.

Frank, M., Marx, D., Nedelkovski, V., Pahr, D. H., & Thurner, P. J. (2018). Dehydration of individual bovine trabeculae causes transition from ductile to quasi-brittle failure mode. *Journal of the mechanical behavior of biomedical materials*, *87*, 296-305.

Fratzl, P., Schreiber, S., & Klaushofer, K. (1996). Bone mineralization as studied by small-angle X-ray scattering. *Connective tissue research*, *34*(4), 247-254.

Fratzl, P., & Weinkamer, R. (2007). Nature's hierarchical materials. *Progress in Materials Science*, *52*(8), 1263-1334. https://doi.org/https://doi.org/10.1016/j.pmatsci.2007.06.001

Fritsch, A., & Hellmich, C. (2007). 'Universal'microstructural patterns in cortical and trabecular, extracellular and extravascular bone materials: micromechanics-based prediction of anisotropic elasticity. *Journal of Theoretical Biology*, *244*(4), 597-620.

Fritsch, A., Hellmich, C., & Dormieux, L. (2009). Ductile sliding between mineral crystals followed by rupture of collagen crosslinks: experimentally supported micromechanical explanation of bone strength. *Journal of theoretical biology*, *260*(2), 230-252.

Gautieri, A., Buehler, M. J., & Redaelli, A. (2009). Deformation rate controls elasticity and unfolding pathway of single tropocollagen molecules. *Journal of the Mechanical Behavior of Biomedical Materials*, *2*(2), 130-137. https://doi.org/https://doi.org/10.1016/j.jmbbm.2008.03.001

Gautieri, A., Vesentini, S., Montevecchi, F. M., & Redaelli, A. (2008). Mechanical properties of physiological and pathological models of collagen peptides investigated via steered molecular dynamics simulations. *Journal of Biomechanics*, *41*(14), 3073-3077. https://doi.org/https://doi.org/10.1016/j.jbiomech.2008.06.028

Gautieri, A., Vesentini, S., Redaelli, A., & Buehler, M. J. (2011). Hierarchical structure and nanomechanics of collagen microfibrils from the atomistic scale up. *Nano letters*, *11*(2), 757-766.

Ghanbari, J., & Naghdabadi, R. (2009). Nonlinear hierarchical multiscale modeling of cortical bone considering its nanoscale microstructure. *Journal of biomechanics*, *42*(10), 1560-1565.

Grant, C. A., Brockwell, D. J., Radford, S. E., & Thomson, N. H. (2008). Effects of hydration on the mechanical response of individual collagen fibrils. *Applied Physics Letters*, *92*(23), 233902.

Habelitz, S., Balooch, M., Marshall, S. J., Balooch, G., & Marshall, G. W. (2002). In situ atomic force microscopy of partially demineralized human dentin collagen fibrils. *Journal of Structural Biology*, *138*(3), 227-236. https://doi.org/https://doi.org/10.1016/S1047-8477(02)00029-1

Hambli, R. (2011). Apparent damage accumulation in cancellous bone using neural networks. *Journal of the Mechanical Behavior of Biomedical Materials*, *4*(6), 868-878. https://doi.org/https://doi.org/10.1016/j.jmbbm.2011.03.002

Hambli, R., & Barkaoui, A. (2012). Physically based 3D finite element model of a single mineralized collagen microfibril. *Journal of Theoretical Biology*, *301*, 28-41. https://doi.org/https://doi.org/10.1016/j.jtbi.2012.02.007

Hamed, E., Lee, Y., & Jasiuk, I. (2010). Multiscale modeling of elastic properties of cortical bone. *Acta mechanica*, *213*(1), 131-154.

Hang, F., & Barber, A. H. (2011). Nano-mechanical properties of individual mineralized collagen fibrils from bone tissue. *Journal of the Royal Society Interface*, *8*(57), 500-505.

Harley, R., James, D., Miller, A., & White, J. W. (1977). Phonons and the elastic moduli of collagen and muscle. *Nature*, *267*, 285. https://doi.org/10.1038/267285a0

Hassenkam, T., Fantner, G. E., Cutroni, J. A., Weaver, J. C., Morse, D. E., & Hansma, P. K. (2004). High-resolution AFM imaging of intact and fractured trabecular bone. *Bone*, *35*(1), 4-10.

Hellmich, C., Barthélémy, J.-F., & Dormieux, L. (2004). Mineral–collagen interactions in elasticity of bone ultrastructure–a continuum micromechanics approach. *European Journal of Mechanics-A/Solids*, *23*(5), 783-810.

Hellmich, C., & Ulm, F.-J. (2002). Micromechanical model for ultrastructural stiffness of mineralized tissues. *Journal of engineering mechanics*, *128*(8), 898-908.

Hengsberger, S., Kulik, A., & Zysset, P. (2002). Nanoindentation discriminates the elastic properties of individual human bone lamellae under dry and physiological conditions. *Bone*, *30*(1), 178-184.

Hill, R. (1963). Elastic properties of reinforced solids: some theoretical principles. *Journal of the Mechanics and Physics of Solids*, *11*(5), 357-372.
Hofmann, H., Voss, T., Kühn, K., & Engel, J. (1984). Localization of flexible sites in thread-like molecules from electron micrographs: Comparison of interstitial, basement membrane and intima collagens. *Journal of Molecular Biology*, *172*(3), 325-343. https://doi.org/https://doi.org/10.1016/S0022-2836(84)80029-7
Jaeger, C., Groom, N. S., Bowe, E. A., Horner, A., Davies, M. E., Murray, R. C., & Duer, M. J. (2005). Investigation of the Nature of the Protein− Mineral Interface in Bone by Solid-State NMR. *Chemistry of materials*, *17*(12), 3059-3061.
Jonvaux, J., Hoc, T., & Budyn, E. (2012). Analysis of micro fracture in human Haversian cortical bone under compression. *International journal for numerical methods in biomedical engineering*, *28*(9), 974-998.
Jäger, I., & Fratzl, P. (2000). Mineralized collagen fibrils: a mechanical model with a staggered arrangement of mineral particles. *Biophysical journal*, *79*(4), 1737-1746.
Kalliauer, J., Kahl, G., Scheiner, S., & Hellmich, C. (2020). A new approach to the mechanics of DNA: Atoms-to-beam homogenization. *Journal of the Mechanics and Physics of Solids*, *143*, 104040.
Kraiem, T., Barkaoui, A., Chafra, M., Hambli, R., & Tavares, J. M. R. S. (2017). New three-dimensional model based on finite element method of bone nanostructure: single TC molecule scale level. *Computer Methods in Biomechanics and Biomedical Engineering*, *20*(6), 617-625. https://doi.org/10.1080/10255842.2017.1280734
Law, J., Parsons, J., Silver, F., & Weiss, A. (1989). An evaluation of purified reconstituted type 1 collagen fibers. *Journal of biomedical materials research*, *23*(9), 961-977.
Lees, S., Prostak, K., Ingle, V., & Kjoller, K. (1994). The loci of mineral in turkey leg tendon as seen by atomic force microscope and electron microscopy. *Calcified Tissue International*, *55*(3), 180-189.
Lorenzo, A. C., & Caffarena, E. R. (2005). Elastic properties, Young's modulus determination and structural stability of the tropocollagen molecule: a computational study by steered molecular dynamics. *Journal of Biomechanics*, *38*(7), 1527-1533. https://doi.org/https://doi.org/10.1016/j.jbiomech.2004.07.011
Maghsoudi-Ganjeh, M., Wang, X., & Zeng, X. (2020). Computational investigation of the effect of water on the nanomechanical behavior of bone. *Journal of the mechanical behavior of biomedical materials*, *101*, 103454.
Martínez-Reina, J., Domínguez, J., & García-Aznar, J. M. (2011). Effect of porosity and mineral content on the elastic constants of cortical bone: a multiscale approach. *Biomechanics and Modeling in Mechanobiology*, *10*(3), 309-322. https://doi.org/10.1007/s10237-010-0236-4
Mori, T., & Tanaka, K. (1973). Average stress in matrix and average elastic energy of materials with misfitting inclusions. *Acta metallurgica*, *21*(5), 571-574.
Mouss, M. E., Rekik, A., Zellagui, S., Merzouki, T., & Hambli, R. (2020). Numerical modeling of the effects hydration and number of hydrogen bonds on the mechanical properties of the tropocollagen molecule. *Proceedings of the Institution of Mechanical Engineers, Part H: Journal of Engineering in Medicine*, 0954411919898935.
Nagaraja, S., Lin, A. S. P., & Guldberg, R. E. (2007). Age-related changes in trabecular bone microdamage initiation. *Bone*, *40*(4), 973-980. https://doi.org/https://doi.org/10.1016/j.bone.2006.10.028
Nemat-Nasser, S., & Hori, M. (2013). *Micromechanics: overall properties of heterogeneous materials*. Elsevier.
Nemat-Nasser, S., Yu, N., & Hori, M. (1993). Bounds and estimates of overall moduli of composites with periodic microstructure. *Mechanics of materials*, *15*(3), 163-181.
Nestler, F. H. M., Hvidt, S., Ferry John, D., & Veis, A. (1983). Flexibility of collagen determined from dilute solution viscoelastic measurements. *Biopolymers*, *22*(7), 1747-1758. https://doi.org/10.1002/bip.360220710

Nomura, S., Hiltner, A., Lando, J., & Baer, E. (1977). Interaction of water with native collagen. *Biopolymers: Original Research on Biomolecules*, *16*(2), 231-246.

Nyman, J. S., Gorochow, L. E., Horch, R. A., Uppuganti, S., Zein-Sabatto, A., Manhard, M. K., & Does, M. D. (2013). Partial removal of pore and loosely bound water by low-energy drying decreases cortical bone toughness in young and old donors. *Journal of the mechanical behavior of biomedical materials*, *22*, 136-145.

Nyman, J. S., Roy, A., Shen, X., Acuna, R. L., Tyler, J. H., & Wang, X. (2006). The influence of water removal on the strength and toughness of cortical bone. *Journal of biomechanics*, *39*(5), 931-938.

Persikov, A. V., Ramshaw, J. A. M., Kirkpatrick, A., & Brodsky, B. (2000). Amino Acid Propensities for the Collagen Triple-Helix. *Biochemistry*, *39*(48), 14960-14967. https://doi.org/10.1021/bi001560d

Pham, T. T., Lemaire, T., Capiez-Lernout, E., Lewerenz, M., To, Q.-D., Christie, J. K., . . . Naili, S. (2015). Properties of water confined in hydroxyapatite nanopores as derived from molecular dynamics simulations. *Theoretical Chemistry Accounts*, *134*(5), 59.

Pidaparti, R., Chandran, A., Takano, Y., & Turner, C. (1996). Bone mineral lies mainly outside collagen fibrils: predictions of a composite model for osternal bone. *Journal of biomechanics*, *29*(7), 909-916.

Privalov, P. L. (1982). Stability of Proteins: Proteins which do not Present a Single Cooperative System. In C. B. Anfinsen, J. T. Edsall, & F. M. Richards (Eds.), *Advances in Protein Chemistry* (Vol. 35, pp. 1-104). Academic Press. https://doi.org/https://doi.org/10.1016/S0065-3233(08)60468-4

Ramachandran, G., & Kartha, G. (1955). Structure of collagen. *Nature*, *176*(4482), 593.

Ramachandran, G. N. (1956). Structure of Collagen. *Nature*, *177*, 710. https://doi.org/10.1038/177710b0

Ramachandran, G. N., & Kartha, G. (1954). Structure of Collagen. *Nature*, *174*, 269. https://doi.org/10.1038/174269c0

Raspanti, M., Congiu, T., & Guizzardi, S. (2001). Tapping-mode atomic force microscopy in fluid of hydrated extracellular matrix. *Matrix biology : journal of the International Society for Matrix Biology*, *20*(8), 601-604. https://doi.org/10.1016/s0945-053x(01)00174-3

Reilly, D. T., & Burstein, A. H. (1975). The elastic and ultimate properties of compact bone tissue. *Journal of biomechanics*, *8*(6), 393-405.

Remaggi, F., Canè, V., Palumbo, C., & Ferretti, M. (1998). Histomorphometric study on the osteocyte lacuno-canalicular network in animals of different species. I. Woven-fibered and parallel-fibered bones. *Italian journal of anatomy and embryology= Archivio italiano di anatomia ed embriologia*, *103*(4), 145-155.

Rho, J.-Y., Kuhn-Spearing, L., & Zioupos, P. (1998). Mechanical properties and the hierarchical structure of bone. *Medical Engineering & Physics*, *20*(2), 92-102. https://doi.org/https://doi.org/10.1016/S1350-4533(98)00007-1

Rho, J.-Y., & Pharr, G. M. (1999). Effects of drying on the mechanical properties of bovine femur measured by nanoindentation. *Journal of Materials Science: Materials in Medicine*, *10*(8), 485-488.

Rho, J. Y., Roy, M. E., Tsui, T. Y., & Pharr, G. M. (1999). Elastic properties of microstructural components of human bone tissue as measured by nanoindentation. *Journal of Biomedical Materials Research: An Official Journal of The Society for Biomaterials, The Japanese Society for Biomaterials, and The Australian Society for Biomaterials*, *45*(1), 48-54.

Rho, J. Y., Zioupos, P., Currey, J. D., & Pharr, G. M. (2002). Microstructural elasticity and regional heterogeneity in human femoral bone of various ages examined by nano-indentation. *Journal of biomechanics*, *35*(2), 189-198.

ROBINSON, R. A., & ELLIOTT, S. R. (1957). The Water Content of Bone: I. The Mass of Water, Inorganic Crystals, Organic Matrin, and" CO: 2: Space" Components in a Unit Volume of Dog Bone. *JBJS*, *39*(1), 167-188.

Rosen, V. B., Hobbs, L., & Spector, M. (2002). The ultrastructure of anorganic bovine bone and selected synthetic hyroxyapatites used as bone graft substitute materials. *Biomaterials*, *23*(3), 921-928.

Saito, M., & Marumo, K. (2010). Collagen cross-links as a determinant of bone quality: a possible explanation for bone fragility in aging, osteoporosis, and diabetes mellitus. *Osteoporosis International*, *21*(2), 195-214. https://doi.org/10.1007/s00198-009-1066-z

Samuel, J., Park, J.-S., Almer, J., & Wang, X. (2016). Effect of water on nanomechanics of bone is different between tension and compression. *Journal of the mechanical behavior of biomedical materials*, *57*, 128-138.

Sansalone, V., Lemaire, T., & Naili, S. (2009). Variational homogenization for modeling fibrillar structures in bone. *Mechanics Research Communications*, *36*(2), 265-273.

Sasaki, N., & Enyo, A. (1995). Viscoelastic properties of bone as a function of water content. *Journal of Biomechanics*, *28*(7), 809-815.

Sasaki, N., & Odajima, S. (1996). Stress-strain curve and young's modulus of a collagen molecule as determined by the X-ray diffraction technique. *Journal of Biomechanics*, *29*(5), 655-658. https://doi.org/https://doi.org/10.1016/0021-9290(95)00110-7

Sasaki, N., & Sudoh, Y. (1997). X-ray pole figure analysis of apatite crystals and collagen molecules in bone. *Calcified tissue international*, *60*(4), 361-367.

Sedlin, E. D., & Hirsch, C. (1966). Factors affecting the determination of the physical properties of femoral cortical bone. *Acta Orthopaedica Scandinavica*, *37*(1), 29-48.

Shen, Z. L., Dodge, M. R., Kahn, H., Ballarini, R., & Eppell, S. J. (2008). Stress-strain experiments on individual collagen fibrils. *Biophysical journal*, *95*(8), 3956-3963.

Shoulders, M. D., & Raines, R. T. (2009). COLLAGEN STRUCTURE AND STABILITY. *Annual review of biochemistry*, *78*, 929-958. https://doi.org/10.1146/annurev.biochem.77.032207.120833

Siegmund, T., Allen, M. R., & Burr, D. B. (2008). Failure of mineralized collagen fibrils: modeling the role of collagen cross-linking. *Journal of biomechanics*, *41*(7), 1427-1435.

Silver, F. H., Christiansen, D., Snowhill, P. B., Chen, Y., & Landis, W. J. (2000). The role of mineral in the storage of elastic energy in turkey tendons. *Biomacromolecules*, *1*(2), 180-185.

Smith, J., & Walmsley, R. (1959). Factors affecting the elasticity of bone. *Journal of anatomy*, *93*(Pt 4), 503.

Sun, C. T., & Li, S. (1988). Three-dimensional effective elastic constants for thick laminates. *Journal of Composite Materials*, *22*(7), 629-639.

Sun, Y.-L., Luo, Z.-P., Fertala, A., & An, K.-N. (2002). Direct quantification of the flexibility of type I collagen monomer. *Biochemical and Biophysical Research Communications*, *295*(2), 382-386. https://doi.org/https://doi.org/10.1016/S0006-291X(02)00685-X

Suvorov, A. P., & Dvorak, G. J. (2002). Rate form of the Eshelby and Hill tensors. *International Journal of Solids and Structures*, *39*(21-22), 5659-5678.

Tommasini, S. M., Nasser, P., Schaffler, M. B., & Jepsen, K. J. (2009). Relationship Between Bone Morphology and Bone Quality in Male Tibias: Implications for Stress Fracture Risk. *Journal of Bone and Mineral Research*, *20*(8), 1372-1380. https://doi.org/10.1359/JBMR.050326

Townsend, P. R., Rose, R. M., & Radin, E. L. (1975). Buckling studies of single human trabeculae. *Journal of biomechanics*, *8*(3-4), 199-201.

Turner, C. H., Rho, J., Takano, Y., Tsui, T. Y., & Pharr, G. M. (1999). The elastic properties of trabecular and cortical bone tissues are similar: results from two microscopic measurement techniques. *Journal of biomechanics*, *32*(4), 437-441.

Unal, M., & Akkus, O. (2015). Raman spectral classification of mineral-and collagen-bound water's associations to elastic and post-yield mechanical properties of cortical bone. *Bone*, *81*, 315-326.

Unal, M., Yang, S., & Akkus, O. (2014). Molecular spectroscopic identification of the water compartments in bone. *Bone*, *67*, 228-236.

Ural, A., & Mischinski, S. (2013). Multiscale modeling of bone fracture using cohesive finite elements. *Engineering Fracture Mechanics*, *103*, 141-152.

Van Der Rijt, J. A., Van Der Werf, K. O., Bennink, M. L., Dijkstra, P. J., & Feijen, J. (2006). Micromechanical testing of individual collagen fibrils. *Macromolecular bioscience*, *6*(9), 697-702.

Vercher, A., Giner, E., Arango, C., Tarancón, J. E., & Fuenmayor, F. J. (2014). Homogenized stiffness matrices for mineralized collagen fibrils and lamellar bone using unit cell finite element models. *Biomechanics and modeling in mechanobiology*, *13*(2), 437-449.

Vercher-Martínez, A., Giner, E., Arango, C., & Fuenmayor, F. J. (2015). Influence of the mineral staggering on the elastic properties of the mineralized collagen fibril in lamellar bone. *Journal of the mechanical behavior of biomedical materials*, *42*, 243-256.

Verz, xe, & r, F. (1963). The Aging of Collagen. *Scientific American*, *208*(4), 104-117.

Verzár, F. (1969). The Stages and Consequences of Ageing of Collagen. *Gerontology*, *15*(2-3), 233-239. https://doi.org/10.1159/000211689

Vesentini, S., Fitié, C. F. C., Montevecchi, F. M., & Redaelli, A. (2005). Molecular assessment of the elastic properties of collagen-like homotrimer sequences. *Biomechanics and Modeling in Mechanobiology*, *3*(4), 224-234. https://doi.org/10.1007/s10237-004-0064-5

Viguet-Carrin, S., Garnero, P., & Delmas, P. D. (2006). The role of collagen in bone strength. *Osteoporosis International*, *17*(3), 319-336. https://doi.org/10.1007/s00198-005-2035-9

Wallace, J. M., Rajachar, R. M., Allen, M. R., Bloomfield, S. A., Robey, P. G., Young, M. F., & Kohn, D. H. (2007). Exercise-Induced Changes in the Cortical Bone of Growing Mice Are Bone and Gender Specific. *Bone*, *40*(4), 1120-1127. https://doi.org/10.1016/j.bone.2006.12.002

Weinberger, C., & Cai, W. (2004). Lecture Note 2. Eshelby's Inclusion I. In: Stanford University.

Weiner, S., & Wagner, H. D. (1998). The material bone: structure-mechanical function relations. *Annual review of materials science*, *28*(1), 271-298.

Wenger, M. P., Bozec, L., Horton, M. A., & Mesquida, P. (2007). Mechanical properties of collagen fibrils. *Biophysical journal*, *93*(4), 1255-1263.

Wolfram, U., Wilke, H.-J., & Zysset, P. K. (2010). Rehydration of vertebral trabecular bone: influences on its anisotropy, its stiffness and the indentation work with a view to age, gender and vertebral level. *Bone*, *46*(2), 348-354.

Yan, J., Daga, A., Kumar, R., & Mecholsky, J. J. (2008). Fracture toughness and work of fracture of hydrated, dehydrated, and ashed bovine bone. *Journal of biomechanics*, *41*(9), 1929-1936.

Yang, L., van der Werf, K. O., Koopman, B. F., Subramaniam, V., Bennink, M. L., Dijkstra, P. J., & Feijen, J. (2007). Micromechanical bending of single collagen fibrils using atomic force microscopy. *Journal of Biomedical Materials Research Part A*, *82*(1), 160-168.

Yoon, H. S., & Katz, J. L. (1976). Ultrasonic wave propagation in human cortical bone—II. Measurements of elastic properties and microhardness. *Journal of biomechanics*, *9*(7), 459-464.

Yoon, Y., Yang, G., & Cowin, S. (2002). Estimation of the effective transversely isotropic elastic constants of a material from known values of the material's orthotropic elastic constants. *Biomechanics and modeling in mechanobiology*, *1*(1), 83-93.

Yoon, Y. J., & Cowin, S. C. (2008a). An estimate of anisotropic poroelastic constants of an osteon. *Biomechanics and Modeling in Mechanobiology*, *7*(1), 13-26. https://doi.org/10.1007/s10237-006-0071-9

Yoon, Y. J., & Cowin, S. C. (2008b). The estimated elastic constants for a single bone osteonal lamella. *Biomechanics and Modeling in Mechanobiology*, *7*(1), 1-11. https://doi.org/10.1007/s10237-006-0072-8

Yuan, F., Stock, S. R., Haeffner, D. R., Almer, J. D., Dunand, D. C., & Brinson, L. C. (2011). A new model to simulate the elastic properties of mineralized collagen fibril. *Biomechanics and modeling in mechanobiology*, *10*(2), 147-160.

Zhang, D., Chippada, U., & Jordan, K. (2007). Effect of the structural water on the mechanical properties of collagen-like microfibrils: a molecular dynamics study. *Annals of biomedical engineering*, *35*(7), 1216-1230.

Zhang, W., Liao, S., & Cui, F. (2003). Hierarchical self-assembly of nano-fibrils in mineralized collagen. *Chemistry of Materials*, *15*(16), 3221-3226.

Zysset, P. K., Guo, X. E., Hoffler, C. E., Moore, K. E., & Goldstein, S. A. (1999). Elastic modulus and hardness of cortical and trabecular bone lamellae measured by nanoindentation in the human femur. *Journal of biomechanics*, *32*(10), 1005-1012.